

Not Just a Dot: the complex UV morphology and underlying properties of Little Red Dots

P. RINALDI,^{1,2,*} N. BONAVENTURA,^{1,*} G. H. RIEKE,¹ S. ALBERTS,¹ K. I. CAPUTI,^{2,3} W. M. BAKER,^{4,5,6} S. BAUM,⁷
R. BHATAWDEKAR,⁸ A. J. BUNKER,⁹ S. CARNIANI,¹⁰ E. CURTIS-LAKE,¹¹ F. D'EUGENIO,^{12,13} E. EGAMI,¹ Z. JI,¹
B. D. JOHNSON,¹⁴ K. HAINLINE,¹ J. M. HELTON,¹ X. LIN,^{15,1} J. LYU,¹ Z. MA,¹ R. MAIOLINO,^{12,16,17}
P. G. PÉREZ-GONZÁLEZ,¹⁸ M. RIEKE,¹ B. E. ROBERTSON,¹⁹ I. SHIVAEI,¹⁸ M. STONE,¹ Y. SUN,¹ S. TACCHELLA,^{12,13}
H. ÜBLER,²⁰ C. C. WILLIAMS,²¹ C. N. A. WILLMER,¹ C. WILLOTT,²² J. ZHANG,¹ AND Y. ZHU¹

¹Steward Observatory, University of Arizona, 933 North Cherry Avenue, Tucson, AZ 85721, USA

²Kapteyn Astronomical Institute, University of Groningen, P.O. Box 800, 9700AV Groningen, The Netherlands

³Cosmic Dawn Center (DAWN), Copenhagen, Denmark

⁴Kavli Institute for Cosmology, University of Cambridge, Madingley Road, Cambridge, CB3 0HA, UK

⁵Cavendish Laboratory - Astrophysics Group, University of Cambridge, 19 JJ Thomson Avenue, Cambridge, CB3 0HE, UK

⁶DARK, Niels Bohr Institute, University of Copenhagen, Jagtvej 128, DK-2200 Copenhagen, Denmark

⁷Department of Physics and Astronomy, University of Manitoba, Winnipeg, MB R3T 2N2, Canada

⁸European Space Agency (ESA), European Space Astronomy Centre (ESAC), Camino Bajo del Castillo s/n, 28692 Villanueva de la Cañada, Madrid, Spain

⁹Department of Physics, University of Oxford, Denys Wilkinson Building, Keble Road, Oxford OX13RH, UK

¹⁰Scuola Normale Superiore, Piazza dei Cavalieri 7, I-56126 Pisa, Italy

¹¹Centre for Astrophysics Research, Department of Physics, Astronomy and Mathematics, University of Hertfordshire, Hatfield AL10 9AB, UK

¹²Kavli Institute for Cosmology, University of Cambridge, Madingley Road, Cambridge, CB3 0HA, UK

¹³Cavendish Laboratory, University of Cambridge, 19 JJ Thomson Avenue, Cambridge, CB3 0HE, UK

¹⁴Center for Astrophysics | Harvard & Smithsonian, 60 Garden St., Cambridge MA 02138 USA

¹⁵Department of Astronomy, Tsinghua University, Beijing 100084, China

¹⁶Cavendish Laboratory - Astrophysics Group, University of Cambridge, 19 JJ Thomson Avenue, Cambridge, CB3 0HE, UK

¹⁷Department of Physics and Astronomy, University College London, Gower Street, London WC1E 6BT, UK

¹⁸Centro de Astrobiología (CAB), CSIC-INTA, Cra. de Ajalvir Km. 4, 28850- Torrejón de Ardoz, Madrid, Spain

¹⁹Department of Astronomy and Astrophysics, University of California, Santa Cruz, 1156 High Street, Santa Cruz, CA 95064, USA

²⁰Max-Planck-Institut für extraterrestrische Physik (MPE), Gießenbachstraße 1, 85748 Garching, Germany

²¹NSF National Optical-Infrared Astronomy Research Laboratory, 950 North Cherry Avenue, Tucson, AZ 85719, USA

²²NRC Herzberg, 5071 West Saanich Rd, Victoria, BC V9E 2E7, Canada

Submitted to ApJ

ABSTRACT

We analyze 99 photometrically selected Little Red Dots (LRDs) at $z \approx 4 - 8$ in the GOODS fields, leveraging ultra-deep JADES NIRCcam short-wavelength (SW) data. We examine the morphology of 30 LRDs; the remaining 69 are predominantly compact, i.e. are strongly dominated by sources $\lesssim 400$ pc in diameter and lack extended components even in stacked SW band images. Among the LRDs selected for morphological analysis, 50% show at least two distinct, associated sources or galaxy components, while the others appear as single sources with highly asymmetric structures. We find median stellar masses of $\log_{10}(M_*/M_\odot) = 9.07^{+0.11}_{-0.08}$ for pure stellar models with $A_V \approx 1.16^{+0.11}_{-0.21}$ mag, and $\log_{10}(M_*/M_\odot) = 9.67^{+0.17}_{-0.27}$ for models including AGNs, where $A_V \approx 2.74^{+0.55}_{-0.71}$ mag, consistent with recent results showing LRDs tend to have high stellar masses and dust content when fitted with AGN models. NIRSspec spectra are available for 15 sources, 6 of which fall within the morphological analysis sample and show multiple components. Among these 15, broad H α emission is detected in 40%, with full-width half-maximum (FWHM) ranging from 1200 to 2900 km/s. One source exhibits

broad $H\beta$ emission with $\text{FWHM} = 2000 \pm 500$ km/s. Analysis of line ratios probing the interstellar medium (ISM) reveals a composite nature, indicating AGN activity combined with stellar processes. These findings suggest LRDs have a mixed nature, with AGN signatures in some cases linked to disturbed morphologies observed at rest-frame UV wavelengths.

Keywords: Active galactic nuclei(16); High-redshift galaxies (734); Galaxy evolution (594); Near infrared astronomy (1093)

1. INTRODUCTION

With its unparalleled sensitivity and angular resolution at infrared (IR) wavelengths, JWST (Gardner et al. 2023) has opened new frontiers for exploring the early Universe. Not only has it provided the opportunity to study well-known high-redshift galaxies previously discovered with the Hubble Space Telescope (HST), such as GN-z11 (Bouwens et al. 2010; Oesch et al. 2016), in much greater detail (e.g., Bunker et al. 2023; Maiolino et al. 2024a; Tacchella et al. 2023), but it has also revealed whole populations of high-redshift galaxies (e.g., Bradley et al. 2023). One of these groundbreaking discoveries is the identification of very compact and red sources, initially reported by Labbé et al. (2023a) and subsequently termed “Little Red Dots” (LRDs) by Matthee et al. (2024).

These sources are characterized by (1) their compactness in the F444W band and (2) their red color at observed wavelengths greater than $\approx 2 \mu\text{m}$ —covered by the Near Infrared Camera (NIRCam; Rieke et al. 2023) Long Wavelength (LW) channel. They exhibit a distinct Spectral Energy Distribution (SED) marked by clear Lyman and Balmer breaks, and the unique and famous “v-shaped” SED in the $\lambda - f_\lambda$ plane; i.e., their continua are relatively blue in the rest ultraviolet but become very red approaching the rest optical.

At the very beginning, these sources were reported to exhibit uncomfortably large stellar masses ($M_\star > 10^{10} M_\odot$) with a large amount of dust ($A_V > 1.5$ mag; see Labbé et al. 2023a).

Over time, various alternative explanations have been proposed to address these puzzling results. In some cases, the issue could simply arise from an error in the redshift estimation, as demonstrated, e.g., by Kocevski et al. (2023a) for one of the massive galaxies identified by Labbé et al. (2023a) and Pérez-González et al. (2023a).

Another potential solution explains the high M_\star values by invoking prominent nebular emission, which could mimic the observed red colors at $\lambda > 2 \mu\text{m}$. Recent studies based on JWST observations have indeed shown high-z galaxies with a prominent ($H\beta + [\text{OIII}]$)

complex and/or $H\alpha$ emission lines (e.g., Endsley et al. 2023; Rinaldi et al. 2023; Boyett et al. 2024; Caputi et al. 2024; Endsley et al. 2024; Rinaldi et al. 2024). Therefore, if strong emission lines are present, the stellar masses could decrease by a factor of 10, as recently reported by Desprez et al. (2024).

Because of their puzzling nature, the discovery of the LRDs has triggered, in less than two years, a vast amount of literature (e.g., Furtak et al. 2023; Labbé et al. 2023a,b; Killi et al. 2023; Kokorev et al. 2023; Übler et al. 2023; Akins et al. 2024; Barro et al. 2024; Durodola et al. 2024; Greene et al. 2024; Kocevski et al. 2024; Kokorev et al. 2024a,b; Kokubo & Harikane 2024; Iani et al. 2024; Hainline et al. 2024a; Matthee et al. 2024; Pérez-González et al. 2024; Williams et al. 2024), leading to one of the most intriguing questions in extragalactic astronomy today: *What is the nature of LRDs?*

As observations continue, both photometric and spectroscopic, different groups have tried to unveil the true nature of these red and compact sources. Some of them exhibit broad ($\approx 1000 \text{ km s}^{-1}$) $H\alpha$ emission lines (Killi et al. 2023; Kokorev et al. 2023; Kocevski et al. 2023a; Greene et al. 2024; Matthee et al. 2024); therefore, it is widely believed that LRDs could potentially host active galactic nuclei (AGNs). However, their SED model fits can be ambiguous, leaving it unclear whether the emission is primarily driven by an AGN or star formation (Barro et al. 2024). It is also possible that LRDs are a mixed population with both AGN and star formation-dominated members (e.g., Pérez-González et al. 2024). Interestingly, Pérez-González et al. (2024) report that only 17% of their photometrically selected LRDs present broad spectral components.

It has become evident that the Mid-Infrared Instrument (MIRI; Wright et al. 2023) on board JWST could be a game-changer in studying these objects at MIR wavelengths, as it could tip the scale in distinguishing between stellar and AGN emission. Noteworthy are several studies in this regard, including those by Williams et al. (2024) and Pérez-González et al. (2024), which suggest that these sources could be either dusty starbursts or obscured AGNs. Particularly, Williams et al. (2024), by making use of the Systematic Mid-infrared Instrument Legacy Extragalactic Survey (SMILES; Al-

* These authors contributed equally to this work.

berts et al. 2024) data, found that the average SED of LRDs flattens beyond $5 \mu\text{m}$, indicating the expected turnover of a normal stellar SED at approximately $1.6 \mu\text{m}$ rest-frame. Building upon these findings, Pérez-González et al. (2024) further concluded that the true nature of the LRDs cannot be uniquely described by a single phenomenon, but rather they are likely to be a non-uniform population of objects, with some being extreme starburst galaxies, some dust-obscured AGNs, and some a combination of both.

In this paper, we propose a new approach to advancing our understanding of LRDs. Although these sources are consistently termed “Little Red Dots” due to their selection as red and compact objects in the F444W band from NIRCcam, here we focus on their morphology at observed wavelengths shorter than $2 \mu\text{m}$, leveraging the superior spatial resolution offered by the NIRCcam short-wavelength (SW) channel. Out of a sample of 99 LRDs, we find that 30 (30%) are sufficiently extended and have enough signal-to-noise (SNR) per pixel in the rest-frame ultra-violet (UV) for morphological analysis. The remaining 70% appear predominantly compact ($\lesssim 400 \text{ pc}$), likely due to their low SNR in each individual band, which prevents the characterization of any extended components, even when stacking the SW bands. While earlier studies have investigated this subject (e.g., Killi et al. 2023; Baggen et al. 2024), ours is the first to apply a statistical approach to address it.

Given that our LRD sample spans $z \approx 4-8$, the NIRCcam SW bands trace the UV emission from the galaxies, which can include, for example, star-forming clumps and complexes (e.g., Guo et al. 2015) with strong contributions from massive O-, B-, and A-type stars (see e.g., Buta 2011; Rubinur et al. 2024), and potentially also the UV continuum emission from an unobscured AGN accretion disk or outflow. This contrasts with the more-common morphology studies conducted in the rest-optical, where galaxy-scale asymmetries and strong disturbances are conventionally attributed to merging activity, as this wavelength range primarily traces the emission from relatively evolved stars. We therefore complement the rest-UV morphological analysis where possible with additional data from broadband SEDs and spectroscopy, to place our sample of LRDs into the context of previous studies.

The paper is organized as follows. Section 2 describes the datasets and outlines our sample selection. In Section 3, we explain the methodology for analyzing the UV morphological properties of the selected LRDs. Section 4 presents the SED fitting configuration used to derive stellar properties and discusses these results. In Section 5, we examine the spectral properties of the LRD candi-

dates with NIRSspec spectra, followed by an analysis of the morphology of the LRD showing broad Balmer lines in Section 6. Finally, Section 7 provides a summary and discussion of our findings.

Throughout this paper, we consider a cosmology with $H_0 = 70 \text{ km s}^{-1} \text{ Mpc}^{-1}$, $\Omega_M = 0.3$, and $\Omega_\Lambda = 0.7$. All magnitudes are total and refer to the AB system (Oke & Gunn 1983). A Kroupa (2001) initial mass function (IMF) is assumed ($0.1-100 M_\odot$).

2. DATASET & SAMPLE SELECTION

2.1. Dataset

In this study, we utilized data from both JWST and HST in the GOODS-North and GOODS-South fields (Giavalisco et al. 2004; hereafter GOODS-N and GOODS-S).

2.1.1. NIRCcam

We made use of NIRCcam data from JADES/NIRCcam Data Release 2 (JADES DR2 – PIDs: 1180, 1210; PIs.: D. Eisenstein, N. Luetzgendorf; Eisenstein et al. 2023a,b), which includes observations from the JWST Extragalactic Medium-band Survey (JEMS – PID: 1963; PIs: C. C. Williams, S. Tacchella, M. Maseda; Williams et al. 2023) for GOODS-S and the First Reionization Epoch Spectroscopically Complete Observations (FRESCO – PID: 1895; PI: P. Oesch; Oesch et al. 2023) for both GOODS-N and GOODS-S. Additionally, we incorporated NIRCcam data from JADES Data Release 3 (DR3) for GOODS-N (D’Eugenio et al. 2024).

The JADES/NIRCcam data allow us to cover a wide range in wavelengths ($\approx 1 \mu\text{m} - 5 \mu\text{m}$). Specifically, the dataset in GOODS-N allows us to make use of 11 NIRCcam bands (both medium- and broad bands; $0.9 \mu\text{m} - 4.44 \mu\text{m}$), while the dataset in GOODS-S allows us to make use of 14 bands (both medium- and broad bands; $0.9 \mu\text{m} - 4.80 \mu\text{m}$).

We estimate a 5σ depth ranging from 30.5 to 30.9 mag (measured in a $0.2''$ radius circular aperture) for the NIRCcam data in GOODS-S, highlighting that JADES is one of the deepest NIRCcam surveys on the sky¹. On the other hand, we estimate a 5σ depth ranging from 29.3 to 29.9 mag (measured in a $0.2''$ radius circular aperture) for the NIRCcam data in GOODS-N. The total area covered by NIRCcam in the GOODS fields is approximately 124 square arcmin².

¹ Only matched in depth (in some bands) by the MIDIS/NIRCcam-parallel project (Pérez-González et al. 2023b) and The Next Generation Deep Extragalactic Exploratory Public Near-Infrared Slitless Survey (NGDEEP; Bagley et al. 2024)

² The JADES data can be downloaded from the following link: <https://archive.stsci.edu/hlsp/jades>;

2.1.2. *HST*

For the HST data, we utilized ACS/WFC and WFC3/IR data from the Hubble Legacy Field (HLF) observations that cover both fields, GOODS-N and GOODS-S. The HLF provides deep imaging in 9 HST bands covering a wide range of wavelengths (0.4–1.6 μm), from the optical (ACS/WFC F435W, F606W, F775W, F814W, and F850LP filters) to the near-infrared (WFC3/IR F105W, F125W, F140W and F160W filters). We refer the reader to Whitaker et al. (2019) for a more detailed description of these observations³.

2.1.3. *NIRSpec*

We made use of the Near Infrared Spectrograph’s Micro-Shutter Array (NIRSpec/MSA; ??) for the spectroscopic observations from the JADES NIR-Cam+NIRSpec program (PID: 1181, PI: Eisenstein), which cover the spectral range 0.6–5.3 μm , including observations with both the low-dispersion prism ($R = 30\text{--}300$) and all three medium-resolution gratings ($R = 500\text{--}1500$). We refer the reader to D’Eugenio et al. (2024) for a more detailed description of this dataset.

2.2. *Sample Selection*

The ultra-deep NIRC*am* images from JADES in both GOODS-N and GOODS-S enable the photometric selection of red and compact sources, commonly referred to as LRDs, over a total area of ≈ 124 arcmin². The extensive data, ranging from HST to NIRC*am* (the latter also offering medium bands), ensures robustness in photometric redshift estimation (see D’Eugenio et al. 2024; Hainline et al. 2024b). To select our sample of LRDs in the GOODS fields, we made use of the public JADES DR2/DR3 catalogues. For both our selection and SED fitting, we made use of aperture photometry with $r = 0.25''$ (i.e., CIRC3).

Since the initial identification of red and compact sources by Labbé et al. (2023a), significant efforts have been made to refine the photometric selection of LRDs. The selection criteria are reasonably effective in identifying broad-line (BL) AGNs. Greene et al. (2024) found that, of the sources followed up spectroscopically, approximately 60% (9/15) were confirmed as BL AGNs. However, 20% of the candidate sources were brown dwarfs, indicating that an additional criterion against this type of contaminant is needed.

The spectra gathered so far of LRDs (e.g., Kocevski et al. 2023a; Kokorev et al. 2023; Furtak et al. 2023;

Greene et al. 2024; Matthee et al. 2024) reveal a defining feature: their SEDs appear blue at 1–2 μm (1000–2000 \AA rest-frame) and red at 3–5 μm (3100–5200 \AA rest-frame), the so-called “v-shape”. With this in mind, and following the approach presented in Kokorev et al. (2024a), we adopt another color criterion (named **brown dwarf removal**) that can potentially help in reducing the contamination from brown dwarfs, a result based on UNCOVER spectra (see Greene et al. 2024).

In addition, compared to the original selection, we relaxed the criterion regarding adjacent filters to avoid excluding potential LRDs due to possible errors in the photometric measurements. Therefore, we visually inspected *all* selected sources and their SEDs⁴ to ensure the inclusion of genuinely red and compact objects, without misclassification due to strong emission lines.

As demonstrated in various studies, using only color criteria can lead to the selection of red sources, whether they are true LRDs (i.e. red and compact) or red and extended. “Compactness” by itself is arbitrary. Therefore, following the example of recent works (e.g., Pérez-González et al. 2024; Kokorev et al. 2024a), we included a compactness criterion in the F444W band, which is the band that truly defines these sources as red. Specifically, we adopted the following criterion: $F444W(0.5'')/F444W(0.25'') < 1.7$ (aperture diameters).

Thus, the criteria we adopted in this work are as follows:

- **blue slope:** $F150W - F200W < 0.8$ mag
- **red slope:** $F277W - F444W > 0.7$ mag
- **brown dwarf removal:** $F115W - F200W > -0.5$ mag
- **compactness:** $F444W(0.5'')/F444W(0.25'') < 1.7$

We then restricted our selection to galaxies with photometric (or spectroscopic) redshifts within the range of $\approx 4 - 8$. This allowed us, for sources with $F444W \lesssim 28$ mag, to probe the UV part of the rest-frame spectrum of these sources with the SW bands from NIRC*am* (probing 0.2 to 0.4 μm at $z \approx 4$ and 0.1 to 0.2 μm at $z \approx 8$).

By applying the above color and compactness criteria, we initially selected 2677 candidates. After a thorough visual inspection of each source and its SED from EAZY (see Hainline et al. 2024b for more details), we robustly identified 99 photometrically confirmed LRDs

³ The HLF imaging is available at <https://archive.stsci.edu/prepds/hlf/>;

⁴ SEDs come from the official JADES catalogue, where EAZY is adopted; see Hainline et al. (2024b) for more details.

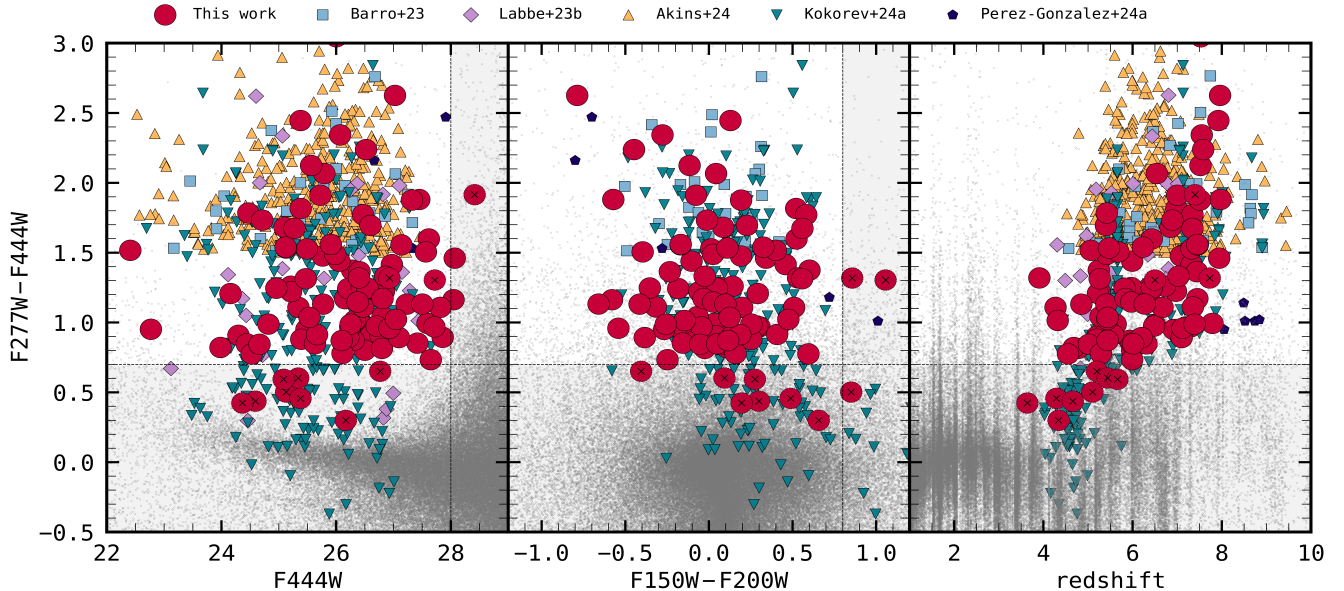


Figure 1. The photometrically selected LRD sample in the GOODS-N and GOODS-S fields at $z \approx 4-8$, alongside other recent literature samples: Labbé et al. (2023a); Akins et al. (2024); Barro et al. (2024); Kokorev et al. (2024a); Pérez-González et al. (2024). Our GOODS-S sample overlaps by 70% with Pérez-González et al. (2024) and by 75% with Kokorev et al. (2024a). The differences arise because Pérez-González et al. (2024) include sources above $z \approx 8$, which we did not consider in this work, and Kokorev et al. (2024a) included sources for which we did not have coverage in both NIRCam/F115W and NIRCam/F200W, preventing us from fully applying our color criteria (see Section 2).

(see Figure 1). This includes 11 sources (marked with a cross) exhibiting LRD-like SEDs that were initially excluded for reasons such as strong emission lines (e.g., the complex $H\beta + [O III]$, which impact the F277W flux at $z \approx 5.5$ and thus the F277W – F444W color), low SNR in the SW bands, incomplete filter coverage (e.g., GS206858, which is missing F150W and F200W), or faintness in F444W. These objects were included to account for their red and compact nature. In addition, 15 of our photometrically selected LRDs have NIRSpec spectra. We show our selection in Figure 1 and list their IDs and coordinates in Table 1⁵. In Figure 2, we present two examples of our selected LRDs where we show the comparison between the NIRCam SW RGB (F090W, F115W, F200W) and the “classic” RGB (F090W, F277W, and F444W). This simple visual comparison reveals that LRDs can exhibit complex morphologies in the UV light, suggesting that *they might not be just a dot*.

We cross-matched our sample with existing AGN catalogues in GOODS-S and GOODS-N. None of our sources appear in the pre-JWST AGN catalogues (Lyu et al. 2022), which is expected given their limited coverage of high-redshift sources. However, six of our sources

are included in the MIRI AGN catalogue presented by Lyu et al. (2024). Among these, four have photometric redshifts consistent with those reported in Lyu et al. (2024), while the remaining two have uncertain redshift estimates. Interestingly, four LRDs (GS197348, GN1001093, GN1061888, and GN1010816) were also identified in Maiolino et al. (2023) and Bunker et al. (2024).

3. LRD MORPHOLOGY

3.1. Morphological analysis: STATMORPH

To study the UV morphology of the LRDs in our sample, we made use of the STATMORPH (Rodríguez-Gomez et al. 2019) software that computes a variety of morphology measures on an input image of a galaxy. To prepare image cutouts for input to the code, for each LRD we generated a $3'' \times 3''$ image stacked over the SW filters⁶, to maximize SNR and ensure meaningful morphological measurements (a STATMORPH measure of > 2.5 SNR/pixel in the source aperture is considered to be trustworthy; refer to Rodríguez-Gomez et al. 2019

⁵ Throughout the paper, we refer to sources by their NIRCam IDs for simplicity.

⁶ For GOODS-S and GOODS-N, we adopted the following filters: F090W, F115W, F150W, F182M, F200W, and F210M. However, we caution that not all these bands were available for every source in our sample due to incomplete coverage in certain filters (e.g., in GOODS-S, F182M and F210M are only available from FRESCO and JEMS data).

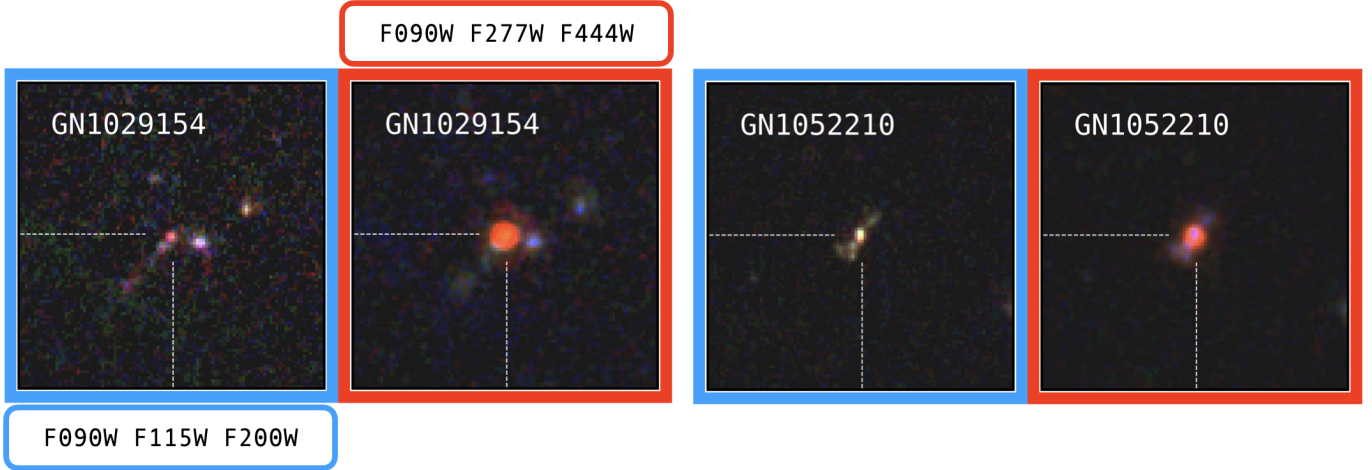


Figure 2. We display two examples from our sample of 99 photometrically selected LRDs in the GOODS-N and GOODS-S fields. For each source, we present two sets of $3'' \times 3''$ RGB postage stamps: one using the SW bands (F090W, F115W, and F200W) and another with the classic RGB colors (F090W, F277W, and F444W). A visual comparison between these two sets reveals that, for these two sources—which also have high SNR in the NIRC2 SW bands—the morphology appears more complex at the shorter wavelengths compared to the classic compact morphology typically associated with LRDs at longer wavelengths (as highlighted in the classic RGB, in red), suggesting that *they are not just a dot*.

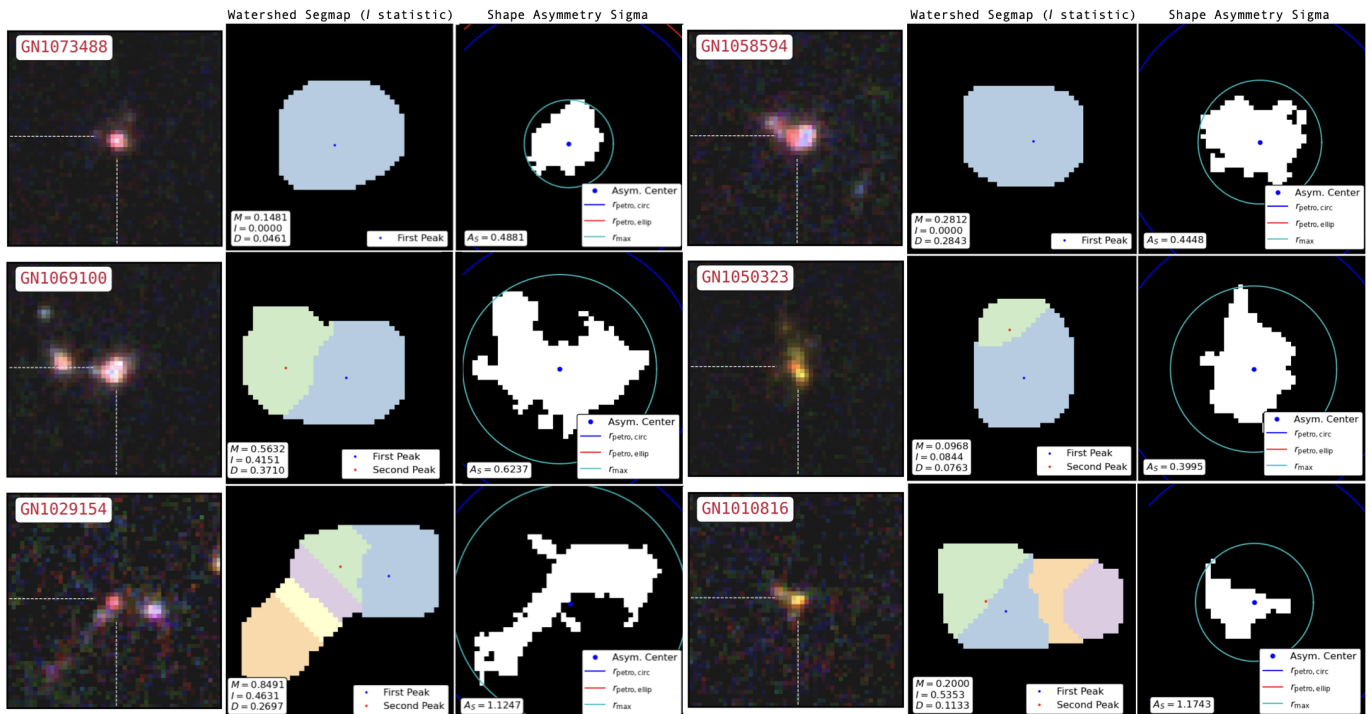


Figure 3. Example STATMORPH output images (middle and rightmost images in each image triplet) along with the associated SW RGB image of galaxy emission (leftmost image), showing the resulting MID and A_S values that comprise our quantitative LRD morphology study. The middle image of each source image triplet shows the segmentation map used specifically to calculate the I statistic, where each distinct intensity maximum is highlighted with a different color. The sources with a single (blue) region represent single sources of emission, however 87% of them show non-zero M statistic values, indicating that the spatial footprints of multiple distinct source regions were detected (see Section 3 and the Appendix for a discussion of the M and I statistics). In the galaxy segmentation image used to calculate shape asymmetry, contained within the r_{max} aperture (cyan line), A_S values greater 0.2 mark a strong asymmetry/disturbance. It can be seen from the representative LRD examples shown here that they present highly asymmetric and complex morphologies, including systems with multiple sources, irregularly shaped single sources with multiple distinct regions of emission, and bright point-like sources embedded in fainter extended emission.

for details). The image stacking also allowed us to iden-

tify the subset definitively showing extended structure

and/or multiple apparently associated sources beyond the size of the SW FWHM. Out of 99 photometrically selected LRDs in GOODS-S and GOODS-N, we find that 30 LRDs in total display clear morphological features (both on the single SW images and the stacked SW bands), while the remaining 69 appear predominantly compact, lacking sufficient SNR for detailed characterization of any extended components, even when stacking the images. After verifying that the resulting subsample of 30 extended LRDs were detected with sufficient SNR/pixel value for analysis (in the range 4.8–12.8), we computed their non-parametric morphological measurements. From among the suite of morphology indicators calculated by STATMORPH, we chose to utilize the non-parametric *multimode-intensity-deviation* (*MID*) statistics (Freeman et al. 2013) and *shape asymmetry* (A_S) parameter (Pawlik et al. 2016).

3.1.1. *Multimode-Intensity-Deviation (MID) and Shape Asymmetry (A_S) Statistics*

The *MID* statistics are useful for detecting multi-component systems, such as the double-nucleus of a late-stage merger; highly disordered post-merger remnants; galaxies with bright star-forming clumps in rest-UV emission; or an apparently single galaxy with an extended emission component(s). Briefly, the multimode (*M*) statistic identifies all non-contiguous groups of image pixels above a given intensity threshold and computes the area ratio of the top two largest regions. The intensity (*I*) statistic complements *M* by calculating the intensity ratio between the two brightest regions in the galaxy image. Finally, the distance (*D*) statistic measures the normalized distance between the brightest local intensity maximum in the galaxy image and the centroid of the total emission, as identified in the binary detection mask (i.e., segmentation map). A more detailed explanation of these statistics can be found in the Appendix. The A_S parameter is a variation of the classic asymmetry parameter (*A*) in that it is calculated using the binary detection mask as opposed to the flux image (Pawlik et al. 2016). The A_S parameter was designed in this way to detect the faint spatial disturbances induced along the edge of a galaxy by merging activity and other galaxy-galaxy interactions, such as wisps, cusps, and tidal tails. In fact, Nevin et al. (2019) show A_S to be the single most important non-parametric diagnostic of merger morphology in imaging data, over a maximal length of the merger lifetime.

Freeman et al. (2013) demonstrate that the *MID* statistics in combination with the classic asymmetry parameter (*A*) represent the most important set of non-parametric morphology indicators for accurately recov-

ering known galaxy classifications⁷, and do not show any systematic variation with galaxy size, degree of elongation, or SNR (at SNR $\gtrsim 1.7$). However, given the unreliability of *A* in instances of relatively low SNR and resolution (e.g. Conselice et al. 2003), as well as its inability to distinguish mergers from non-mergers over a significant fraction of the merger lifetime, we utilize the A_S parameter instead, which outperforms *A* in each of these instances (Nevin et al. 2019).

The detailed algorithmic descriptions of these non-parametric morphology indicators are presented in the Appendix.

3.2. *The UV morphological properties of the LRDs*

In Figure 3, we show the STATMORPH results of the *MID* and A_S statistic computation for a representative subset of the 30 LRDs in our sample appearing as multiple associated sources, irregularly shaped single sources, and apparent point sources embedded in fainter extended emission. In each triplet of images shown per source, the statistic values are displayed along with the corresponding segmentation map used in the calculation of each (Freeman et al. 2013; Pawlik et al. 2016; Rodriguez-Gomez et al. 2019). Figure 4 shows the measured relationship between A_S and the *MID* statistic values, which reveals that all LRDs included in the morphological analysis appear as strongly spatially disturbed systems, independent of the number of distinct sources or emission components detected, as indicated by A_S values greater than 0.2 (Pawlik et al. 2016). It can also be seen that A_S is positively correlated with the corresponding non-zero (i.e., multi-component) *M* and *I* values, as expected where multiple components of emission are detected within/around the source (Freeman et al. 2013; see Appendix for details). Furthermore, the non-zero *M* and *I* statistic values are also positively correlated with one another, showing that the spatial area and brightness of a detected secondary source of emission tend to grow in tandem. The resulting values for the *M* and *I* statistics in our LRD sample show strong cases for multiple associated sources where their values tend towards 1, suggestive of a major merger, as well as candidates for minor mergers where the values are smaller (or one or more significant clumps of UV emission as-

⁷ While the extensively studied *concentration-asymmetry-smoothness* *CAS* (Conselice et al. 2003) and *Gini*– M_{20} (GM_{20}) (Lotz et al. 2004) morphology diagnostics are also computed by STATMORPH, the reliability of these statistics is known to decrease along with decreasing galaxy size and SNR. Therefore, given the compact sizes and high redshift of LRDs, we utilize instead the (*MID*) statistics that were introduced in Freeman et al. (2013) as an alternative to *CAS* and GM_{20} when such criteria hold.

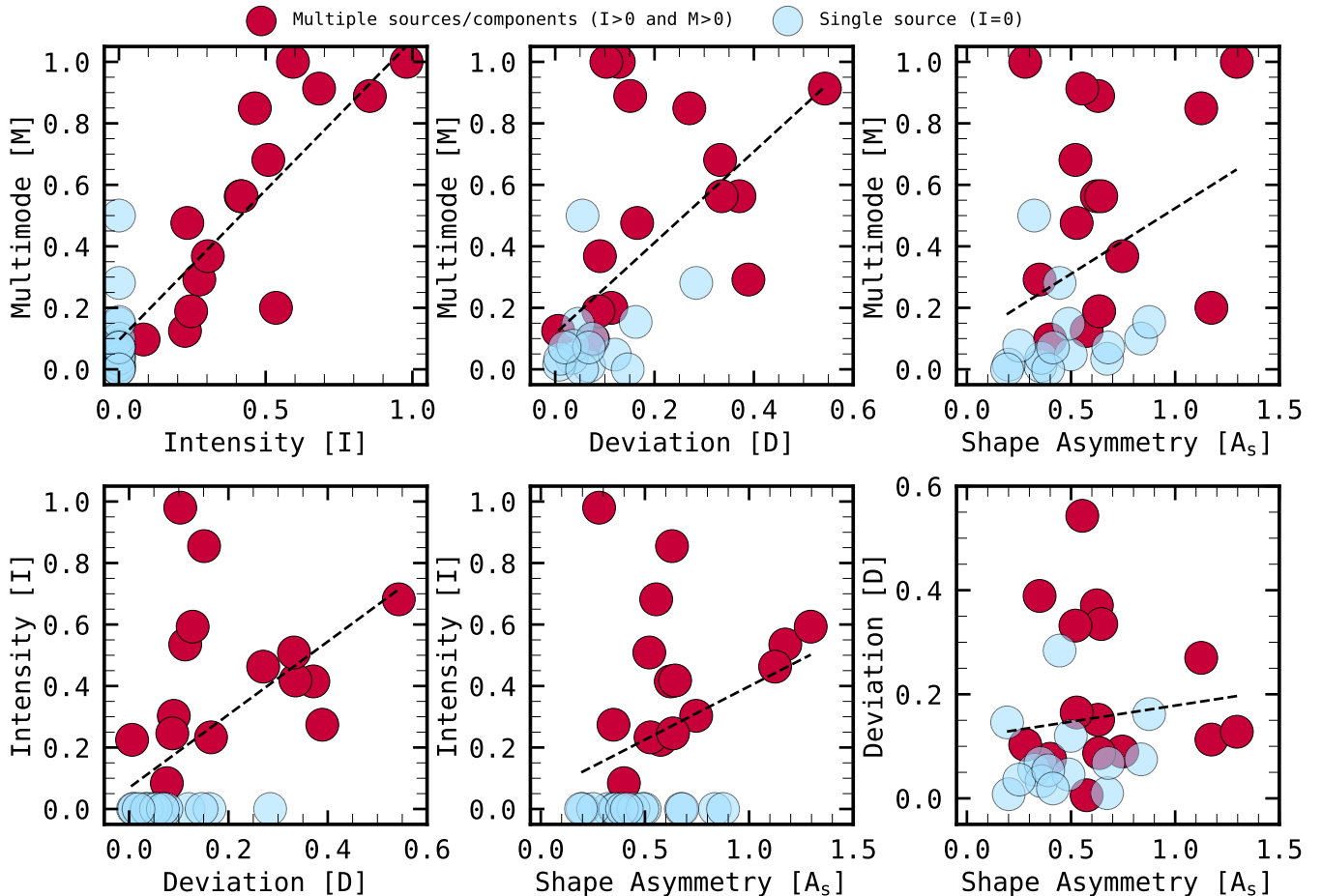


Figure 4. An adaptation of Figure 5 in Freeman et al. (2013), where the *MID* statistics for measuring galaxy morphologies are introduced, but with the classic *asymmetry* parameter, A , replaced by the *shape asymmetry* parameter, A_S ; see Section 3.1. The red symbols are akin to the merger candidates in the referenced work, as they represent the LRDs in our sample exhibiting multiple distinct emission and spatial components (indicated by non-zero I and M values, respectively). Close pairs of sources with similar brightnesses and sizes, such as major-merger candidates, would show I and M values tending towards a value of 1, while lower values of these two statistics would suggest a minor-merger candidate, or a single source with a relatively small and faint ‘companion’ UV clump of emission. The blue symbols represent those LRDs identified with only a single ($I = 0$), asymmetric ($A_S > 0.2$) source of emission, but with most (87%) showing multiple non-contiguous pixel regions by their non-zero M statistic values (similar to the “non-regular” non-merger candidates in Freeman et al. 2013). In short, all of the LRDs examined in the morphological analysis display irregular and extended features. The black lines represent the fit to the multi-source/multi-component LRDs (red points), demonstrating the expected positive linear relationship between these statistics. Based on the random forest regression and classification analysis of the combined *MID* and A statistics measured for 1639 galaxies in HST/WFC3 H - and J -band images in Freeman et al. (2013), both the visually labeled (red) multi-component systems (classified as purely mergers in their study) and the (blue) non-merging irregular galaxies are detected with $\approx 78\%$ accuracy (i.e., the percentage of correctly classified non-regular or merging galaxies).

sociated with a single source). For the $\approx 50\%$ of cases with zero I values (only one intensity peak identified in the galaxy emission) but non-zero M values (multiple non-contiguous pixel groups identified above a given intensity threshold), it is clear from visual inspection that these represent LRDs with a single galaxy attached to an extended asymmetric emission structure. Finally, only in two cases do we find both zero I and M statistic values (i.e., a single and coincident spatial and emission

component). However, both of these sources exhibit an asymmetric/disturbed spatial imprint, one with an A_S value indicative of a mild spatial disturbance, and the other, strong. However, these two LRDs show particularly small sizes and relatively lower SNR compared to the rest of the sample examined in the morphological analysis, making it possible that they have multiple components that evaded detection by M and I .

Given that the D statistic provides an independent measure of galaxy asymmetry (see Appendix) and therefore serves as a non-redundant complement to A_S , we observe these two parameters to positively correlate, as expected, in instances where the LRD appears significantly extended, non-centralized, and disturbed. Furthermore, where a source happens to show a relatively symmetric spatial outline in the A_S binary detection mask with equally weighted pixel values (tending towards lower values of A_S), D can still indicate a relatively high level of disturbance/disorder within the brightness distribution of the corresponding flux image of the galaxy, such as in the observed cases of an extended single source, but with its brightest peak of emission appearing off-center.

In summary, the MID statistics indicate that 50% of the LRDs selected for morphological analysis show at least two distinct, associated sources or galaxy components, with the remainder appearing as single sources with highly asymmetric structure. We also notice from M and I that in $\approx 50\%$ of the multi-component LRDs, the two sources/ regions used in the calculation of each statistic are of comparable brightness and size, suggesting they are potential major-merger candidates in the pre- or late-stage phase. In Table 2, we summarize the main properties estimated with STATMORPH.

4. LRD STELLAR PROPERTIES

4.1. SED Fitting: BAGPIPES

We used BAGPIPES (Carnall et al. 2019) to perform SED fitting and derive the stellar properties of the 99 photometrically selected LRDs. For the 15 galaxies with available spectroscopy, we also performed joint spectrophotometric fitting. In all cases, the redshift was fixed, based on either photometric or spectroscopic values.

BAGPIPES relies on synthetic templates from Bruzual & Charlot (2003) with a Kroupa (2001) IMF, adopting a cut-off mass of $100 M_\odot$, and nebular emission modeled with CLOUDY (Ferland et al. 2013). We employed a continuity non-parametric SFH model (Leja et al. 2019). For the latter, we defined the age bin edges (counted in look-back time from the redshift of the observation) based on each source’s redshift (photometric or spectroscopic), following a logarithmic distribution from $z = 30$ to the age of the Universe at that redshift. We adopted the same approach for the age parameter. Stellar masses were allowed to range between 10^5 and $10^{13} M_\odot$ (uniform prior in log). We opted for a Calzetti reddening law (Calzetti et al. 2000), allowing A_V to vary between 0 and 6, and allowed metallicity (Z/Z_\odot) to range from 0 to 2.5. The ionization parameter (U) was fixed at -2 . Finally, each fit was calculated twice, with and without

invoking an AGN. To set up the AGN contribution, we followed the approach outlined in Carnall et al. (2023) (see their Table 1). We adopted broad, flat (uniform) priors for all parameters.

For the sources with NIRSpec spectra, we followed the techniques described by Carnall et al. (2019) to fully leverage the combination of spectroscopic and photometric data. As outlined in Navarro-Carrera et al. (2024), we allowed for a $< 2\sigma$ perturbation to the spectrum using a second-order Chebyshev polynomial to correct for systematic uncertainties in flux calibration. Additionally, we allow for a multiplicative factor on the spectroscopic errors to correct for underestimated uncertainties.

4.2. Results

For runs allowing AGNs, we find that our LRDs have an average $A_V = 2.74_{-0.71}^{+0.55}$ mag, consistent with the original results from Labbé et al. (2023a), where their sample of red, compact sources exhibited $A_V > 1.5$ mag. This also aligns with the recent findings from Akins et al. (2024), who identified a large population of red, compact objects in COSMOS. Our sources show, on average, $\log_{10}(M_\star/M_\odot) = 9.67_{-0.27}^{+0.17}$, in agreement with the recent literature about LRDs (e.g., Akins et al. 2024; see the left panel in Figure 5). On the other hand, the BAGPIPES run using only stellar models indicates that our LRDs have, on average, $A_V = 1.16_{-0.21}^{+0.11}$ mag and an average $\log_{10}(M_\star/M_\odot) = 9.07_{-0.08}^{+0.11}$. To first order the lower M_\star is a reflection of the lower extinction. These masses may, of course, be overestimated if the galaxies have IMFs that are more top-heavy than the Kroupa one used in BAGPIPES.

Some sources in our sample exhibit very high M_\star (a result consistent also with the runs using stellar models alone), which would require star formation efficiencies (i.e., how effectively gas in molecular clouds is converted into stars over a given period) of $\varepsilon > 0.2$. None of our sources require $\varepsilon > 1$, unlike some of those analyzed in the sample by Akins et al. (2024). Interestingly, among these very massive galaxies, two have NIRSpec spectra and show $\log_{10}(M_\star/M_\odot) > 10$ at $z \approx 6.5 - 7.5$. While one of these has poor-quality NIRSpec data, the other features a high-quality spectrum and still shows a very high M_\star ($\log_{10}(M_\star/M_\odot) = 10.62_{-0.05}^{+0.05}$) at $z_{spec} = 6.759$ (GN1010816). Although such massive objects are rare, they are theoretically expected at such high redshifts. A more detailed analysis of these objects will be presented in a separate paper.

We also estimated the bolometric luminosity (L_{Bol}) for our photometrically selected LRDs. We computed L_{Bol} from the intrinsic best-fit SED (i.e., before any

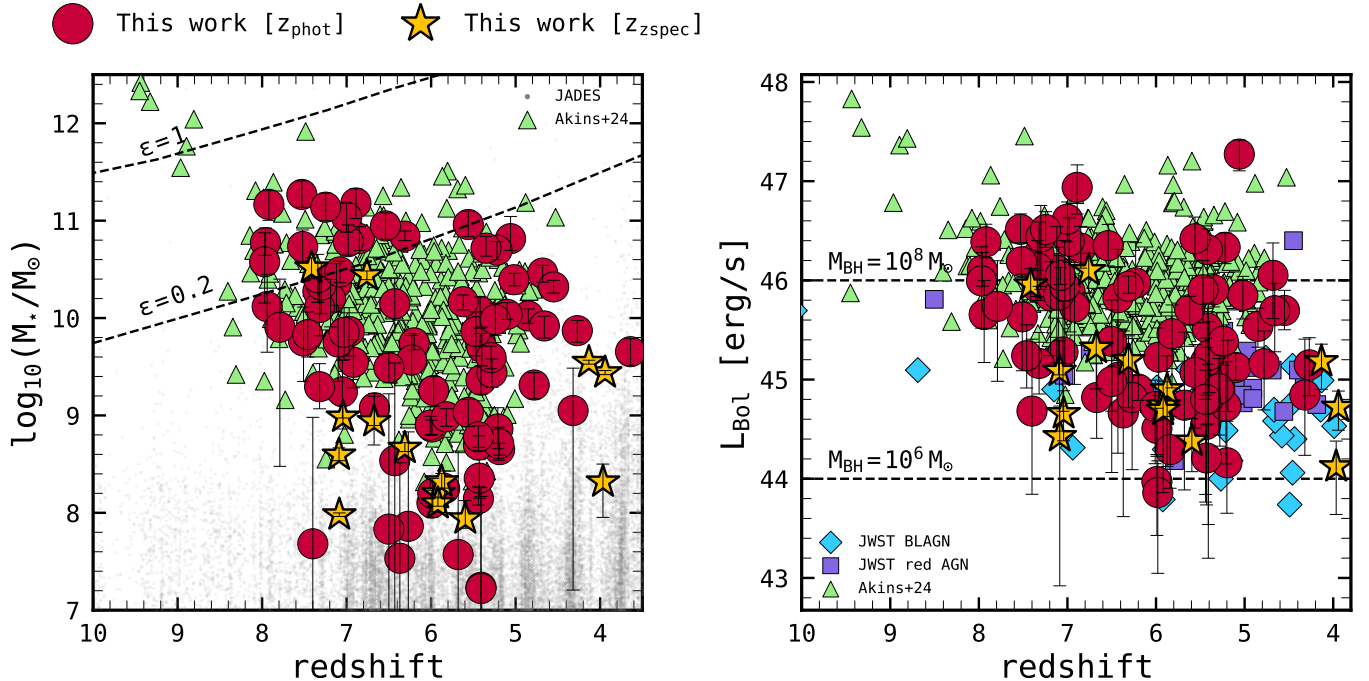


Figure 5. **Left panel:** M_* as a function of redshift for our sample of 99 photometrically selected LRDs in the GOODS fields. In this plot, M_* comes from the BAGPIPES runs with AGN. No significant differences arise when plotting, instead, M_* adopting stellar models only. Gray points represent galaxies from JADES DR2/DR3. The large sample of LRDs from Akins et al. (2024) is presented for comparison. The sources with spectra are denoted by yellow stars. Grey points represent the JADES sources in both GOODS-S and GOODS-N. The allowed M_* as a function of redshift for two different star formation efficiencies values are also shown with black dashed lines. **Right panel:** L_{Bol} as a function of redshift. We computed L_{Bol} from the intrinsic model SED (i.e., before any dust attenuation) by using the monochromatic luminosity at 5100 Å and a bolometric correction of 9 (Richards et al. 2006). For comparison, we plot the LRD sample from Akins et al. (2024) along with some other recent literature, divided into two groups: confirmed BL AGNs (Larson et al. 2023; Harikane et al. 2023; Maiolino et al. 2023; Übler et al. 2023; Bogdan et al. 2024; Maiolino et al. 2024a; Parlanti et al. 2024; Übler et al. 2024) and red AGNs (Kokorev et al. 2023; Furtak et al. 2024; Greene et al. 2024; Matthee et al. 2024). Assuming an Eddington ratio = 1, we show what L_{Bol} would correspond to $\log_{10}(M_{BH}/M_{\odot}) = 6 - 8$ (horizontal dashed lines).

dust attenuation) using the monochromatic luminosity at 5100 Å and applying a bolometric correction of 9 (Richards et al. 2006). In the right panel of Figure 5, we show our sample of LRDs along with recent literature results (Harikane et al. 2023; Maiolino et al. 2023; Larson et al. 2023; Übler et al. 2023; Akins et al. 2024; Bogdan et al. 2024; Furtak et al. 2024; Greene et al. 2024; Kokorev et al. 2024a; Maiolino et al. 2024a; Matthee et al. 2024; Parlanti et al. 2024; Übler et al. 2024). We find that our sample agrees well with the region of parameter space covered by the large LRD sample presented in Akins et al. (2024), with a handful of sources reaching L_{Bol} of up to $\approx 10^{47}$ erg/s.

5. TO BE AN AGN OR NOT TO BE, THAT IS THE QUESTION: INSIGHTS FROM NIRSPEC

Some LRDs show broadening of the Balmer lines, suggesting that they host AGNs (e.g., Greene et al. 2024). To explore their properties, we follow the approach outlined in Kokorev et al. (2024a) to estimate the black hole

mass (M_{BH}) under the assumption that our photometrically selected LRDs are *dominated* by AGNs. In general, a secure determination of M_{BH} is not feasible; however, under this assumption, we can derive an estimate. In the recent literature, the Eddington rate (λ_{Edd}) for confirmed AGN in LRDs was found to range between 10% and 40% (e.g., Kokorev et al. 2023; Furtak et al. 2024; Greene et al. 2024). Following the approach outlined in Kokorev et al. (2024a), we place a lower limit on the M_{BH} by assuming that our AGN candidates accrete at the Eddington limit, i.e., $L_{bol} \approx L_{Edd}$ (where L_{Edd} is directly proportional to M_{BH}). We calculate M_{BH} from the dust-corrected L_{Bol} and find, on average, that $\log_{10}(M_{BH}/M_{\odot}) \approx 7.66^{+0.05}_{-0.15}$. If a significant fraction of the luminosity is derived from star formation, then this lower limit is over-estimated. Using the scaling relation of Greene et al. 2020 from the estimated median stellar mass yields an estimate an order of magnitude smaller. These values are all consistent with the recently discov-

ered population of red and compact sources (e.g., Akins et al. 2024; Kokorev et al. 2024a) and similar to the black hole masses in more traditional AGNs at similar redshift (Harikane et al. 2023; Maiolino et al. 2023). That is, it is plausible that AGNs play an important role in any of our LRDs, including those without spectroscopic evidence for AGNs.

Among our 99 photometrically selected LRDs in the GOODS fields, 15 have NIRSpec spectra, obtained with both the prism and the medium-resolution grating (Bunker et al. 2024; D’Eugenio et al. 2024), including 6 from our fiducial sample with sufficiently high SNR for morphological analysis. Therefore, we explored whether these sources exhibit spectral signatures that could indicate the presence of AGNs. To do so, we made use of a modified version of the MSAEXP line-fitting algorithm (Brammer 2023), which allowed us to measure line fluxes, uncertainties, and observed equivalent widths for both the prism and gratings (Kokorev et al., in prep). We also implemented a custom routine into this code to fit individual (narrow and/or broad) emission lines, deblend them when necessary, and validate the results against MSAEXP. We then excluded one source from our analysis since the quality of its spectra (both prism and medium resolution gratings) prevented us from making proper estimation of any line fluxes. Finally, our findings were cross-matched with the official JADES line emission catalog, showing excellent agreement within the error bars.

Within our sub-sample of LRDs with NIRSpec spectra, we find that 6 (40% of the spectroscopic sample) exhibit significant broadening in the $H\alpha$ emission line (either from prism or grating), with FWHM ranging from approximately 1200 km/s to 2900 km/s, as shown in Figure 6, with 4 of them already presented in previous works (Maiolino et al. 2023; Bunker et al. 2024). Notably, one of these LRDs also shows broadening in the $H\beta$ line (observed with the medium-resolution grating), having $\text{FWHM} \approx 2000 \pm 500$ km/s. We caution the reader that the low resolution of PRISM may lead to significant instrumental broadening (e.g., Greene et al. 2024). Nevertheless, some sources relying solely on PRISM data, such as GS197348, have already been analyzed in previous studies (e.g., Bunker et al. 2023). Three of the LRDs that show broad $H\alpha$ fall in our fiducial sample for morphological analysis. Unfortunately, the other 3 LRDs with broad $H\alpha$ lack sufficient SNR in the NIRCам SW bands (even by stacking the NIRCам SW bands), thus preventing further study of their morphology. Interestingly, one of them, with $\text{SNR} \approx 4-6$ in the NIRCам SW channel (in the central region only), shows a faint component to the NW in F090W and F115W, which however

is too faint to be observed in the stacked NIRCам SW image (F090W, F115W, F150W, F182M, F200W, and F210M).

To investigate further whether the selected LRDs with NIRSpec data could be classified as AGNs, we made use of two diagnostic plots based on the following emission lines: $[\text{OII}]\lambda\lambda 3727, 3728$, $[\text{NeIII}]\lambda 3870$, $H\beta\lambda 4861$, and $[\text{OIII}]\lambda 5007$. In particular, we explored the following ratios: $[\text{OIII}]\lambda 5007/H\beta$ vs. $[\text{NeIII}]\lambda 3870/[\text{OII}]\lambda\lambda 3727$ (commonly referred to as the “OHNO” diagram) and $[\text{OIII}]\lambda 4363/H\gamma$ vs. $[\text{OIII}]\lambda 5007/[\text{OII}]\lambda\lambda 3727$. Below, we present our results.

The OHNO diagram—In the left panel of Figure 7, we analyze our LRD sample by employing the “OHNO” diagram (Trouille et al. 2011; Zeimann et al. 2015; Backhaus et al. 2022, 2023; Cleri et al. 2023; Trump et al. 2023; Feuillet et al. 2024), as the $[\text{NeIII}]\lambda 3870/[\text{OII}]\lambda\lambda 3727, 3728$ ratio has proven to be a robust ionization diagnostic for high-redshift galaxies (e.g., Backhaus et al. 2022, 2023, 2024). This diagnostic is particularly effective because $[\text{NeIII}]\lambda 3870$ and $[\text{OII}]\lambda\lambda 3727, 3728$ have similar ionization energy, and their being very close in wavelength minimizes the effects of dust attenuation. Particularly, it has been shown that employing this ratio can effectively help in distinguishing between star-forming galaxies (SFGs) and AGNs (see Zeimann et al. 2015; Backhaus et al. 2022, 2023, 2024). While this diagram is primarily sensitive to ionization, it also shows a dependence on metallicity (e.g., Tripodi et al. 2024). Therefore, we caution the reader that low-metallicity galaxies may introduce contamination, as already discussed in Scholtz et al. (2023).

On average, our photometrically selected LRDs exhibit $\log_{10}([\text{OIII}]\lambda 5007/H\beta) \gtrsim 0.5$ (median value of 0.71 ± 0.03), with the exception of one source that suffers from poor data quality in both prism and medium-resolution modes. Overall, the members of our sample show a consistently high $[\text{NeIII}]\lambda 3870/[\text{OII}]\lambda\lambda 3727$ ratio compared to the average SFG population. Interestingly, our sample occupies the same region of other LRDs recently studied in the literature (e.g., Killi et al. 2023; Kocevski et al. 2023a; Kokorev et al. 2023; Larson et al. 2023) and, in general, the region occupied by selected broad and/or narrow line AGNs (e.g., Scholtz et al. 2023; Übler et al. 2024). The gray area represents the sample of SFGs and AGNs selected from the Sloan Digital Sky Survey (SDSS) at $z \approx 0$ from York et al. (2000).

The $[\text{OIII}]\lambda 4363/H\gamma$ vs. $[\text{OIII}]\lambda 5007/[\text{OII}]\lambda\lambda 3727$ diagram—In the right panel of Figure 7, we show another diagnostic diagram to investigate the nature of our photometrically selected LRDs: the $[\text{OIII}]\lambda 4363/H\gamma$

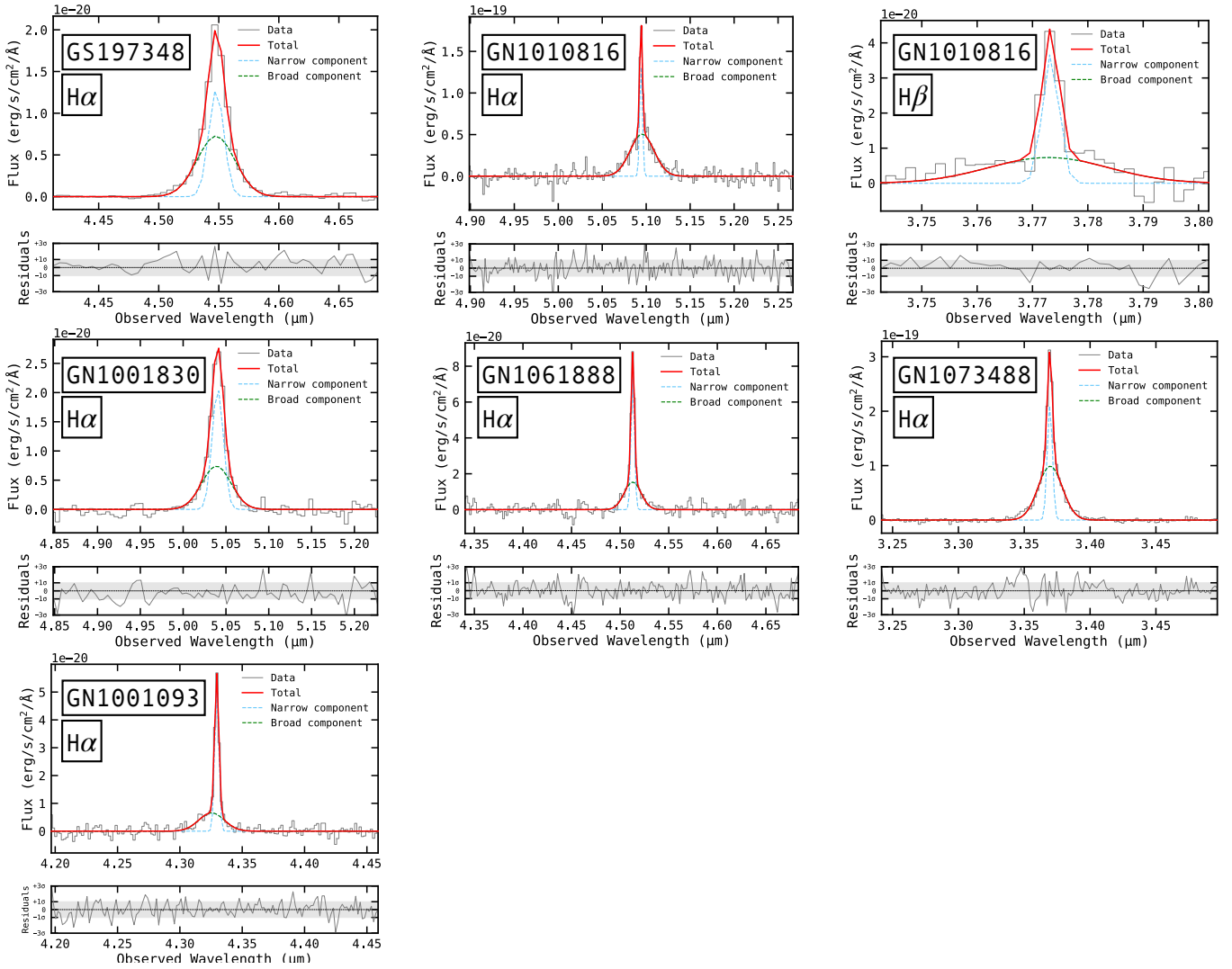


Figure 6. The 6 LRDs that show broadening in their $H\alpha$ from NIRSPEC data (NIRCam IDs, see Table 1): GS197348, GN1010816, GN1001830, GN1061888, and GN1073488. Particularly, GN1010816 (red frame) shows also broadening in its $H\beta$. Some of these objects are already reported in previous works, namely: GS197348, GN1010816, GN1001093, and GN1061888 (Maiolino et al. 2023; Bunker et al. 2024).

vs. $[\text{OIII}]\lambda 5007/[\text{OII}]\lambda 3727$. This diagram has been recently presented in Mazzolari et al. (2024) and, as with the OHNO diagram, offers the advantage of using line ratios that lie very close in wavelength, therefore reducing the effects of dust reddening.

Recent studies have demonstrated that some high-redshift galaxies ($z \gtrsim 8$) exhibit anomalously high $[\text{OIII}]\lambda 4363$ emission, potentially suggesting the presence of an AGN (e.g., Brinchmann 2023). Intriguingly, this trend has been further confirmed by Übler et al. (2024), who suggested that a strong $[\text{OIII}]\lambda 4363/H\gamma$ ratio could actually result from higher interstellar medium (ISM) temperatures driven by AGN activity and, thus, point to the presence of an AGN. We remind the reader that, while this diagnostic is similar to the OHNO diagram, the separation between AGNs and SFGs in this

case is primarily driven by differences in the gas temperature.

As demonstrated by Mazzolari et al. (2024), normal SF galaxies (and their local analogs) tend to populate a well-defined region in this diagram, specifically the lower-right portion of the plot. In contrast, the AGN population spans a broader area, including the upper-left region. In particular, following the discussion presented by Mazzolari et al. (2024) who tested models computed by Gutkin et al. (2016), Feltre et al. (2016), and Nakajima & Maiolino (2022), that area cannot be populated by any SFG model (see their Figure 1b for a more comprehensive view).

The strength of $[\text{OIII}]\lambda 4363$ emission line, which is produced through collisional excitation from high-energy levels, lies in its ability to provide key infor-

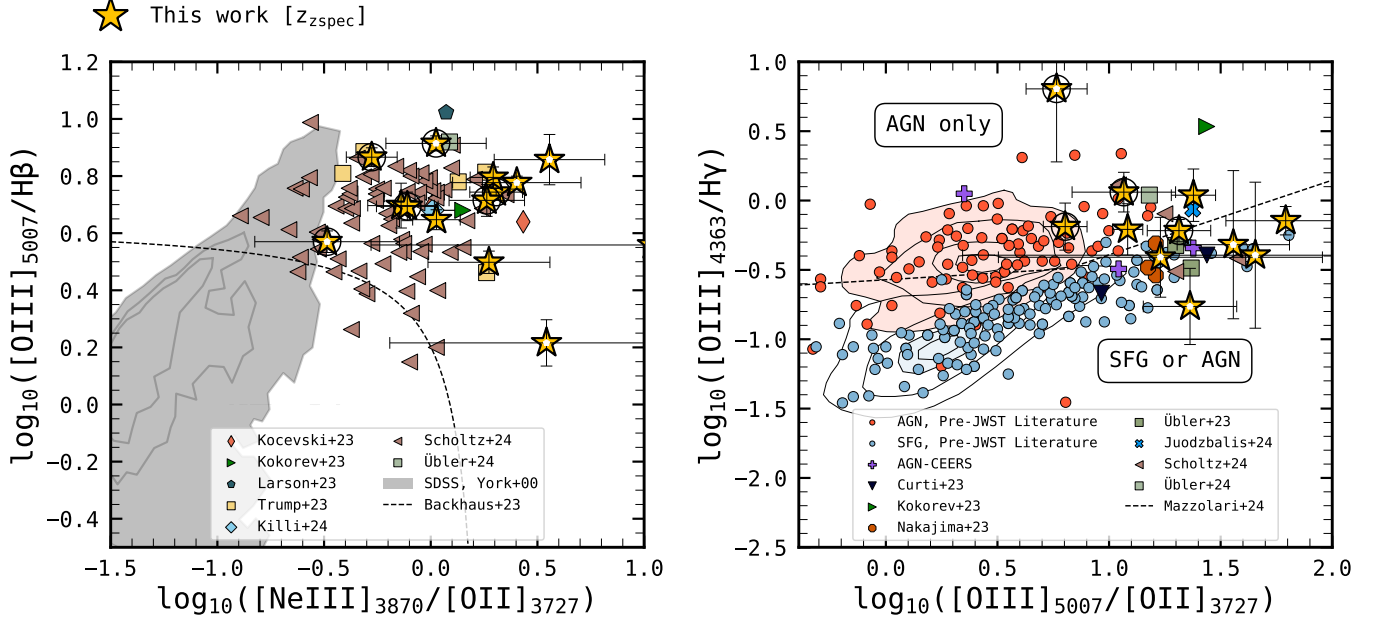


Figure 7. Left Panel: We show the “OHNO” diagram. We present our sources as gold stars along with the recent literature from Kocevski et al. (2023a); Kokorev et al. (2023); Larson et al. (2023); Trump et al. (2023); Killi et al. (2023); Scholtz et al. (2023); Übler et al. (2024). For comparison, we also show the SDSS sample (SFGs and AGNs) at low- z from York et al. (2000). The demarcation line comes from Backhaus et al. (2023). **Right Panel:** We replicate the panel shown in Mazzolari et al. (2024). Our sources are shown as gold stars along with some recent literature: e.g., Curti et al. (2023); Kokorev et al. (2023); Nakajima et al. (2023); Übler et al. (2023); Juodžbalis et al. (2024); Scholtz et al. (2023); Übler et al. (2024). We also show the demarcation line from Mazzolari et al. (2024). Pre-JWST literature for AGNs and SFGs is shown as well (e.g., Izotov et al. 2007; Amorín et al. 2015). The stars marked with black circles are the objects with enough SNR for morphological studies. The sources marked with a white dot are the ones with SNR $\lesssim 2$ for one of the two line ratios involved in these diagnostics.

mation about the gas temperature when compared to the $\text{H}\gamma$ intensity (e.g., Sanders et al. 2016). This ratio can also offer insights into the metallicity of the ISM and the ionization parameter (e.g., Gburek et al. 2019). The primary difference between SFGs and AGNs lies in the source of their ionizing radiation—young star clusters in the former and emission from the accretion disk in the latter—resulting in significantly more powerful ionizing radiation in the case of AGNs. This leads to higher electron temperatures, which, in turn, increase the $[\text{OIII}]\lambda_{4363}$ emission and the $[\text{OIII}]\lambda_{4363}/\text{H}\gamma$ ratio for a given ionization parameter (i.e., the ratio of the number density of incident ionizing photons and the number density of hydrogen atoms).

We observe that six sources lie above the separation line provided by Mazzolari et al. (2024), and, more broadly, they overlap with the sample of AGNs (and some selected LRDs) identified in the recent studies (e.g., Curti et al. 2023; Kokorev et al. 2023; Nakajima et al. 2023; Scholtz et al. 2023; Übler et al. 2023; Juodžbalis et al. 2024; Übler et al. 2024). Notably, one source is placed significantly above the separation line, although we caution the reader that the spectral region of $[\text{OIII}]\lambda_{4363}/\text{H}\gamma$ has low SNR for this source. Inter-

estingly, this source does not exhibit any clear signature of broad components in its Balmer lines, but shows both $[\text{NII}]\lambda_{6548}$ and $[\text{NII}]\lambda_{6583}$ (detected with an SNR of approximately 4–6 in the medium-resolution grating). By inspecting its $[\text{NII}]/\text{H}\alpha$ ratio, we find that this source would lie precisely on the separation line between AGNs and SFGs in the classic “Baldwin, Phillips & Terlevich” (BPT) diagram (Baldwin et al. 1981).

More generally, our sample of photometrically selected LRDs is well constrained within a defined region of the parameter space, which overlaps with the area predominantly populated by recently discovered AGN using JWST. However, we note that this region, just below the demarcation line, also includes a subset of star-forming galaxies (pale blue circles; e.g., Izotov et al. 2007; Amorín et al. 2015; Curti et al. 2023; Nakajima et al. 2023; Scholtz et al. 2023).

Altogether, these two panels highlight the diversity of our LRD sample, ranging from pure AGNs to composite galaxies, underscoring their complex nature as a mix of different ionizing sources, as suggested by previous studies (e.g., Pérez-González et al. 2024). The consistency of our results, with our objects occupying a region

of parameter space shared by AGN-dominated systems and star-forming galaxies, further supports their mixed nature. This suggests that AGN activity might significantly influence the properties of this subset of photometrically selected LRDs, though the extent of this influence remains unclear and warrants deeper spectroscopic investigation. In Table 3, we report the line fluxes estimated for each source.

Finally, we computed M_{BH} for the six sources that show broadening in $H\alpha$ and compared the estimated quantities with the recent literature. To estimate M_{BH} , we followed the approach presented in Reines et al. (2013), for which M_{BH} can be estimated as follows:

$$\log_{10} \left(\frac{M_{BH}}{M_{\odot}} \right) = \alpha + \log_{10}(\varepsilon) + \beta \log_{10} \left(\frac{L_{H\alpha, \text{broad}}}{1 \times 10^{42} \text{ erg/s}} \right) + \gamma \log_{10} \left(\frac{\text{FWHM}_{\text{broad}}}{1 \times 10^3 \text{ km/s}} \right), \quad (1)$$

where, $\alpha = 6.57$, $\beta = 0.47$, and $\gamma = 2.06$.

The results are shown in Figure 8. Overall, our findings align with recent studies of selected LRDs analyzed using spectroscopic data (e.g., Kokorev et al. 2023). They also tend to validate our rough estimates made previously.

6. MORPHOLOGY OF LRDS WITH BROAD $H\alpha$

Among the LRD candidates with NIRSpect spectra, three of them show a sufficiently high SNR and extent for morphological analysis, as well as broad $H\alpha$ (Figure 9). Given the potential for both AGN and star-forming activity that these features imply (in combination with the results of the various spectral line-ratio diagnostics discussed in the previous section), we consider that their highly disturbed appearances may be associated with one or both of these processes, and potentially result from merging activity. As shown in Figure 9, GN1010816 is detected with multiple distinct regions of emission (four, according to its I statistic measure), at least two of which are of comparable intensity and size; and with a total spatial extent measured to have significant asymmetry. Given the sampling of rest-UV emission in the stacked NIRCcam SW-channel images used for morphological characterization, this example could indicate multiple merging galaxies, triggering bursts of star formation in the form of UV clumps (e.g., Guo et al. 2015), and/or one or two unobscured AGN. It is also possible that the multiple components of emission do not represent distinct nuclei in the act of merging, but a single galaxy (possibly in the post-merger phase) with a surrounding clumpy structure from merger- and/or AGN-triggered star formation, and/or clumpy accretion onto an AGN (e.g., DeGraf et al. 2017).

The other two LRDs with broad $H\alpha$ line emission appear as single sources with a highly asymmetric spatial footprint, as determined through both human and computer vision. GN1073488 appears distinctly bright and point-like and is embedded in an asymmetric diffuse structure. GS197348, on other hand, appears elongated, with a relatively long, narrow, and faint emission structure appearing to “shoot off” from one of its sides. This faint extended feature is notably missed by the MID statistics, but is caught by the A_S algorithm, which was explicitly designed to detect such faint edge features. If this feature is real and associated with the LRD - which it appears to be based on its presence in all the NIRCcam SW filters considered - it could potentially be a manifestation of AGN feedback, e.g. the UV emission that has been found to spatially coincide with AGN radio jets (e.g., Rubinur et al. 2024).

7. SUMMARY AND DISCUSSION

In this study, we analyzed a sample of 99 photometrically identified LRDs in the GOODS fields, selected using color and compactness criteria (Figure 1 and 2; e.g., Labbé et al. 2023a).

We examined the rest-wavelength UV morphology of these LRDs by analyzing ultra-deep NIRCcam SW images using the STATMORPH software. Out of 99 photometrically selected LRDs, 30% of them show extended structure and also with sufficient SNR in these bands to allow for a meaningful morphological analysis. The remaining 70% are strongly dominated by sources $\lesssim 400$ pc in diameter and lack extended components even in stacked SW band images. We found that all these objects exhibit $A_S > 0.2$, with a median value of ≈ 0.5 , suggesting that these sources are generally highly spatially disturbed and likely to be undergoing mergers or interactions. Such elevated A_S values align with recent findings (e.g., Bonaventura et al. 2024), which suggest that galaxies with $A_S > 0.2$ are frequently linked to ongoing or recent merger activity (Figure 3 and 4).

While most studies consider the rest-optical emission of galaxies in diagnosing merger morphologies, we have analyzed the rest-UV morphology of LRDs at $z \approx 4 - 8$ imaged in the NIRCcam SW bands. The expectation from the results of Mager et al. (2018) is that the UV asymmetry of merging/peculiar galaxies will be consistent with, or appear more pronounced than, that measured in the rest-optical, for all galaxy types: these authors observe a significant increase in the *clumpiness* of all galaxy types at shorter wavelengths. Furthermore, more recent studies on high- z galaxy morphology have shown that, in general, galaxies do not exhibit dramatic changes when transitioning from UV to optical light.

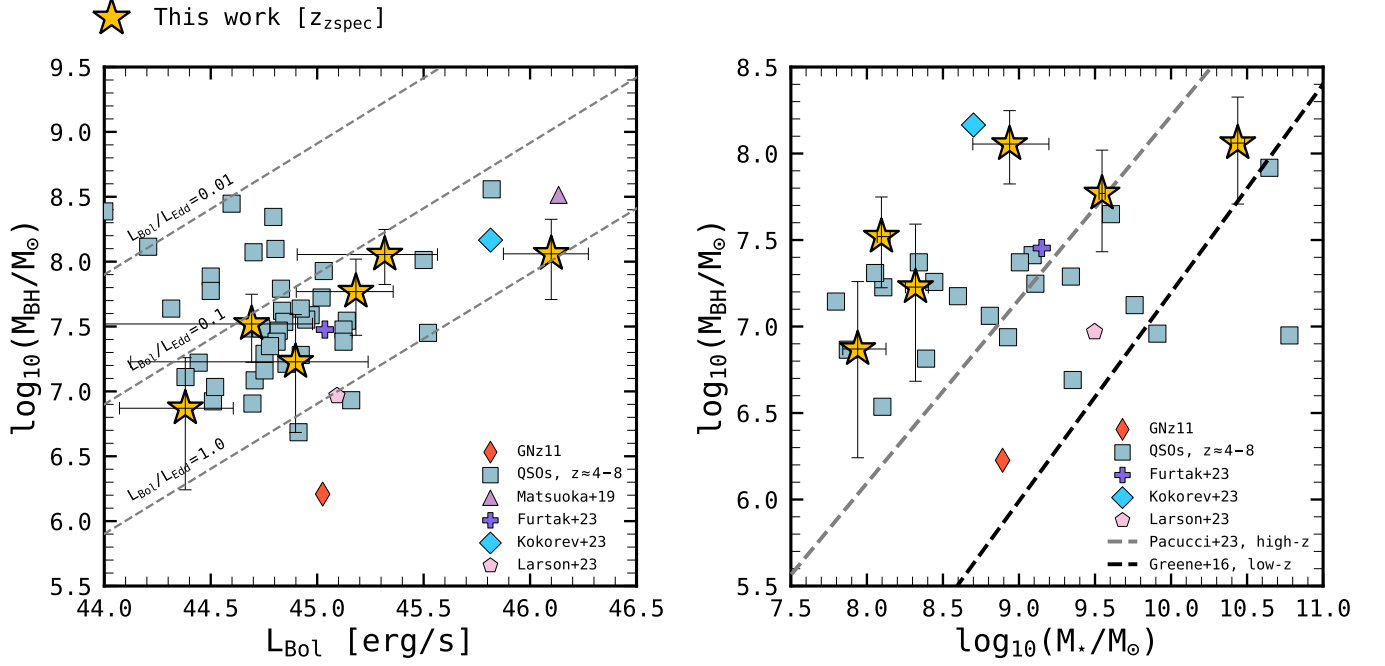


Figure 8. Left panel: The derived black hole mass (M_{BH}) as a function of bolometric luminosity (L_{Bol}), in comparison with recent findings in the literature (e.g., GNz11, CEERS_1019, the triply lensed quasar among others; Matsuoka et al. 2019; Furtak et al. 2023; Harikane et al. 2023; Kocevski et al. 2023a; Kokorev et al. 2023; Larson et al. 2023; Maiolino et al. 2023, 2024a; Matthee et al. 2024). The dashed lines represent bolometric luminosities corresponding to Eddington ratios of $L_{\text{Bol}}/L_{\text{Edd}} = 0.01, 0.1, \text{ and } 1.0$. **Right panel:** The black hole-to-stellar mass relation is presented, with the bold black dashed line indicating the best fit to $z \approx 0$ AGN samples (Greene et al. 2016). The trend at higher redshifts is based on the recent analysis by Pacucci et al. (2023). Color codes and markers are the same as for the left panel.

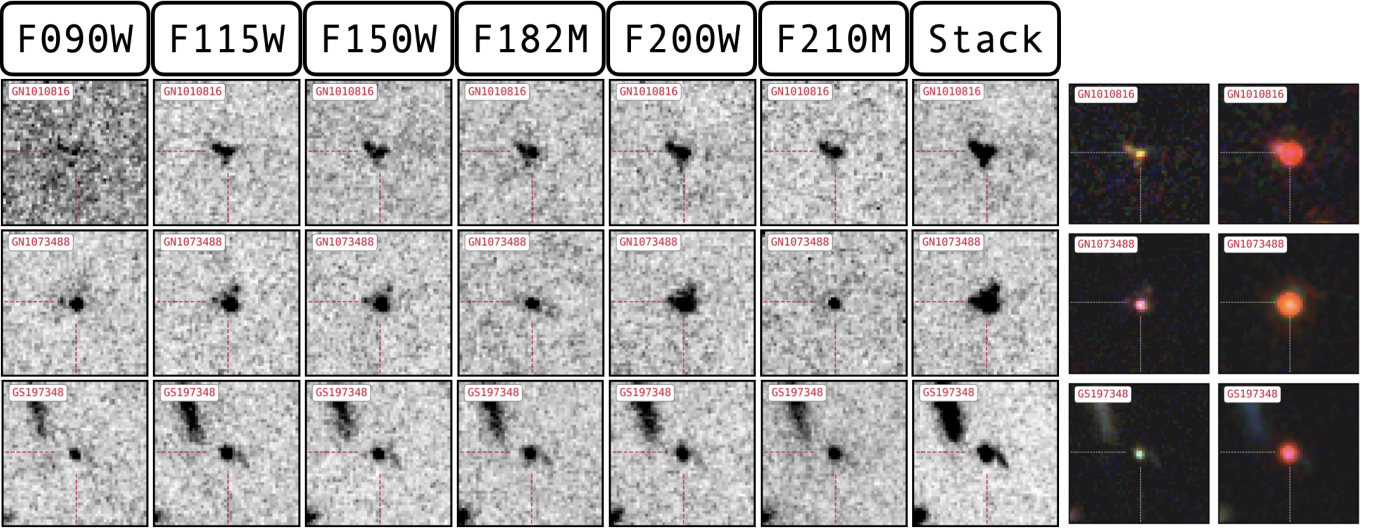


Figure 9. The LRDs in our sample with NIRSpectra that show broad $H\alpha$ line emission (and with sufficient SNR for morphological characterization), possibly indicating the presence of an AGN. Postage stamps ($1.5'' \times 1.5''$) from the NIRCcam SW channel (F090W, F115W, F150W, F182M, F200W, and F210M). For visual comparison, we also show the RGB postage stamps considering the SW bands only and the “classic” RGB (i.e., F090W, F277W, and F444W).

For instance, Treu et al. (2023) studied a sample of Lyman Break Galaxies during the Epoch of Reionization and found that, within the uncertainties and scatter,

the classic morphological indices (G , M_{20} , A , etc.) remain relatively consistent across different wavelengths. That is, the measures of galaxy morphology in our study

should reflect those expected from the rest-optical emission. However, a caveat to consider in the rest-UV is that, without knowledge of the quantity, distribution, optical depth, and covering fraction of the dust present in a galaxy, the extent to which it may be affecting the observed rest-UV morphology cannot be constrained. While it is possible that the presence of severely attenuating dust could contribute to a clumpy UV morphology by blocking from view all but the brightest UV emission regions, it is unlikely that the 30 star-forming LRDs included in our morphological analysis appear with such irregular and extended features purely as a result of this effect.

The disturbed LRD morphology we observe could be driven by gravitational interactions that channel gas toward the central regions, potentially fueling both star formation and black hole growth, finally leading to an AGN phase. However, quite surprisingly, preliminary analysis of the stacked X-ray emission of the LRDs using the deepest available *Chandra* ACIS-I imaging coverage, from the CDFS 7Ms survey, shows no detection; this mirrors the findings of Yue et al. (2024), who were equally baffled by the non-detection of stacked X-ray emission of their LRD sample. Gas accretion onto an AGN should exhibit significant X-ray luminosity, as well as the shock-heated gas of a major, gas-rich galaxy merger (e.g., Cox et al. 2006 and references therein). Therefore, it is conceivable that, in X-ray-undetected LRDs, a dynamical or other physical process is preventing the angular momentum of the gas in the system from dropping low enough to funnel onto the nucleus, causing a delay to the infall of tidal material and the consequent detectable X-ray emission. For instance, several galaxy merger simulations suggest that the higher gas turbulence and velocity dispersion observed in high-redshift galaxies in comparison to their lower-redshift counterparts inhibits the propagation of gas inflows towards the center of the system, possibly resulting in suppressed AGN activity in gaseous, high-redshift galaxies (see Shah et al. 2020 and references therein). In any case, low X-ray luminosity has been found for a variety of other high-redshift AGNs (Lyu et al. 2024; Maiolino et al. 2024b), so the puzzle is not confined to LRDs.

To put the morphology results in context, we employed BAGPIPES to analyze the properties of all 99 LRDs and found that, on average, the sources exhibit $A_V \approx 2.74_{-0.71}^{+0.55}$ mag when AGN models are included, and $A_V \approx 1.16_{-0.21}^{+0.11}$ mag when using stellar models only. The average stellar mass is $\log_{10}(M_*/M_\odot) \approx 9.67_{-0.27}^{+0.17}$, or $\log_{10}(M_*/M_\odot) = 9.07_{-0.08}^{+0.11}$ when stellar models only are considered. To first order, the difference in M_* is a reflection of different dust extinctions. We also es-

timated their (dust-corrected) L_{Bol} from their best-fit spectra (assuming a correction factor of ≈ 9 , Richards et al. 2006). By making the assumption that all these selected LRDs host AGNs and adopting an Eddington ratio of 1, we derived lower limits for their M_{BH} , with a median value of $\log_{10}(M_{BH}/M_\odot) \gtrsim 7.66_{-0.15}^{+0.05}$, or an order of magnitude smaller if we estimate BH masses from the usual relation with the M_* . These results are also consistent with those reported for the recently discovered population of red and compact sources (e.g., Akins et al. 2024; Kokorev et al. 2024a), i.e., our sample is typical of the general class.

Among our sample of LRDs, 15 have NIRSpect spectra, which have been explored to investigate whether they host an AGN. We employed three different diagnostic diagrams to evaluate the state of their ISM. We find a variety of behavior, ranging from those classified as pure AGNs to those showing a mixed nature (i.e., classified as composite galaxies), indicating their complex nature (Figure 7). Interestingly, six of them exhibit broadening in their $H\alpha$ lines, with one also showing broadening in $H\beta$. The remaining 60% show no clear signs of AGN presence (i.e., no broadening in their Balmer lines); nonetheless, the diagnostic plots employed in this study hint at either AGN activity or a mixed nature for these sources, suggesting that deeper spectroscopic data are needed to further investigate their nature. For those showing broad $H\alpha$, we estimated their M_{BH} from the broad $H\alpha$ component (Reines et al. 2013) and found that our results are consistent with recent findings about LRDs (Figure 8; e.g., Furtak et al. 2023; Kokorev et al. 2023; Larson et al. 2023).

A significant portion of our LRD sample exhibits disturbed UV morphology, with some objects clearly observed in a merger state (Figure 9). Two sources with NIRSpect data show very high M_* and highly disturbed UV morphology (Figure 5). The most reliably modeled of these sources shows a very high M_* ($\log_{10}(M_*/M_\odot) = 10.62_{-0.05}^{+0.05}$) at $z_{spec} = 6.759$.

The mechanisms that trigger rapid gas accretion onto super massive black holes (SMBHs) remain still unclear, which directly ties into the nature of the LRDs in our sample. A compelling theoretical hypothesis is that galaxy mergers and interactions drive AGN activity by funneling gas into the central regions of galaxies, thereby fueling the SMBH (e.g., Gabor et al. 2016; Blumenthal & Barnes 2018), also recently supported by Duan et al. (2024). However, observational evidence remains inconclusive, with several studies finding no definitive correlation (e.g., Villforth et al. 2014; Hewlett et al. 2017; Ellison et al. 2019; Kocevski et al. 2023b; Pierce et al. 2023). Given that our morphological analysis revealed

significant asymmetries and signs of disturbance in a substantial fraction of our LRDs, it is plausible that interactions might play a substantial role in triggering AGNs in these systems (although we do not have a control sample to put this on a more quantitative basis). This would be an important, although perhaps not unexpected, difference from the situation at lower redshift. Further spectroscopic and morphological studies, particularly those utilizing deep NIRSpec/IFU data, will be essential in unveiling the true nature of the LRDs and exploring the connection between their disturbed UV morphologies and potential AGN activity.

This work is based on observations made with the NASA/ESA/CSA JWST. The data were obtained from the Mikulski Archive for Space Telescopes at the Space Telescope Science Institute, which is operated by the Association of Universities for Research in Astronomy, Inc., under NASA contract NAS 5-03127 for JWST. These observations are associated with JWST programs GTO #1180, GO #1210, GO #1963, GO #1895, and # 3215. The authors acknowledge the FRESCO, JEMS, and # 3215 teams led by coPIs P. Oesch, C. C. Williams, M. Maseda, D. Eisenstein, and R. Maiolino for developing their observing program with a zero-exclusive-access period. Processing for the JADES NIRCам data release was performed on the lux cluster at the University of California, Santa Cruz, funded by NSF MRI grant AST 1828315. Also based on observations made with the NASA/ESA Hubble Space Telescope obtained from the Space Telescope Science Institute, which is operated by the Association of Universities for Research in Astronomy, Inc., under NASA contract NAS 526555.

KIC acknowledges funding from the Dutch Research Council (NWO) through the award of the Vici Grant VI.C.212.036.

ST acknowledges support by the Royal Society Research Grant G125142.

HÜ acknowledges support through the ERC Starting Grant 101164796 “APEX”.

PGP-G acknowledges support from grant PID2022-139567NB-I00 funded by Spanish Ministerio de Ciencia e Innovación MCIN/AEI/10.13039/501100011033, FEDER, UE.

RM acknowledges support by the Science and Technology Facilities Council (STFC), by the ERC through Advanced Grant 695671 “QUENCH”, and by the UKRI Frontier Research grant RISEandFALL. RM also acknowledges funding from a research professorship from the Royal Society.

SC acknowledges support by European Union’s HE ERC Starting Grant No. 101040227 - WINGS.

WMB acknowledges support by a research grant (VIL54489) from VILLUM FONDEN.

ECL acknowledges support of an STFC Webb Fellowship (ST/W001438/1).

BER acknowledges support from the NIRCам Science Team contract to the University of Arizona, NAS5-02015, and JWST Program 3215.

The research of CCW is supported by NOIRLab, which is managed by the Association of Universities for Research in Astronomy (AURA) under a cooperative agreement with the National Science Foundation.

AJB acknowledges funding from the “FirstGalaxies” Advanced Grant from the European Research Council (ERC) under the European Union’s Horizon 2020 research and innovation program (Grant agreement No. 789056).

MR, CNAW, BDJ, and EE acknowledge the JWST/NIRCам contract to the University of Arizona NAS5-02015.

Table 1. List of the photometrically selected LRDs in the GOODS fields

JADES ID	NIRCam ID	Redshift	R.A. (deg)	Dec. (deg)	JADES ID	NIRCam ID	Redshift	R.A. (deg)	Dec. (deg)
JADES-GN+189.1797+62.2246	1001093	5.595*	189.1797	62.2246	JADES-GS+53.0763-27.9099	2532	6.98	53.0763	-27.9099
JADES-GN+189.0915+62.2281	1001830	6.675*	189.0915	62.2281	JADES-GS+53.1191-27.8926	11786	7.34	53.1191	-27.8926
JADES-GN+189.1096+62.2285	1001895	7.52	189.1096	62.2285	JADES-GS+53.1072-27.8906	13418	6.50	53.1072	-27.8906
JADES-GN+189.1277+62.2326	1002836	7.10	189.1277	62.2326	JADES-GS+53.1136-27.8848	19348	5.41	53.1136	-27.8848
JADES-GN+189.0963+62.2391	1004685	7.414*	189.0963	62.2391	JADES-GS+53.0570-27.8744	35453	5.10	53.0570	-27.8744
JADES-GN+189.1517+62.2594	1010767	6.20	189.1517	62.2594	JADES-GS+53.0641-27.8709	39376	7.00	53.0641	-27.8709
JADES-GN+189.1520+62.2596	1010816	6.759*	189.1520	62.2596	JADES-GS+53.0558-27.8690	41769	7.79	53.0558	-27.8690
JADES-GN+189.2038+62.2684	1013041	7.089*	189.2038	62.2684	JADES-GS+53.1304-27.8607	54648	6.37	53.1304	-27.8607
JADES-GN+189.0571+62.2689	1013188	7.32	189.0571	62.2689	JADES-GS+53.1153-27.8592	57356	4.27	53.1153	-27.8592
JADES-GN+189.0385+62.2693	1013282	7.12	189.0385	62.2693	JADES-GS+53.1083-27.8510	70714	6.50	53.1083	-27.8510
JADES-GN+189.0659+62.2733	1014361	4.32	189.0659	62.2733	JADES-GS+53.0605-27.8484	73690	5.40	53.0605	-27.8484
JADES-GN+189.0721+62.2734	1014406	5.19	189.0721	62.2734	JADES-GS+53.1476-27.8420	79803	5.41	53.1476	-27.8420
JADES-GN+189.0506+62.2794	1016275	7.97	189.0506	62.2794	JADES-GS+53.1127-27.8383	82737	5.21	53.1127	-27.8383
JADES-GN+189.0577+62.2836	1017514	5.02	189.0577	62.2836	JADES-GS+53.0732-27.8331	86916	7.05	53.0732	-27.8331
JADES-GN+189.0612+62.2841	1017694	7.34	189.0612	62.2841	JADES-GS+53.1281-27.8292	89635	5.99	53.1281	-27.8292
JADES-GN+188.9878+62.2911	1020140	4.66	188.9878	62.2911	JADES-GS+53.1338-27.8283	90354	7.96	53.1338	-27.8283
JADES-GN+189.1131+62.2924	1020485	5.26	189.1131	62.2924	JADES-GS+53.1590-27.8183	99267	6.67	53.1590	-27.8183
JADES-GN+189.1590+62.2602	1029154	5.62	189.1590	62.2602	JADES-GS+53.1593-27.8117	104238	5.28	53.1593	-27.8117
JADES-GN+189.0409+62.2693	1030265	5.42	189.0409	62.2693	JADES-GS+53.1019-27.8109	104849	5.24	53.1019	-27.8109
JADES-GN+189.1798+62.2824	1032447	7.086*	189.1798	62.2824	JADES-GS+53.1408-27.8022	110739	5.916*	53.1408	-27.8022
JADES-GN+189.0870+62.2908	1033797	5.22	189.0870	62.2908	JADES-GS+53.1254-27.7874	120484	7.08	53.1254	-27.7874
JADES-GN+189.1983+62.2970	1034762	7.043*	189.1983	62.2970	JADES-GS+53.1269-27.7862	121710	7.92	53.1269	-27.7862
JADES-GN+189.2586+62.1432	1037138	7.51	189.2586	62.1432	JADES-GS+53.1728-27.7831	124327	7.94	53.1728	-27.7831
JADES-GN+189.2395+62.1444	1037341	5.68	189.2395	62.1444	JADES-GS+53.2040-27.7721	132229	7.247*	53.2040	-27.7721
JADES-GN+189.2346+62.1475	1037974	7.46	189.2346	62.1475	JADES-GS+53.1908-27.7679	136872	7.19	53.1908	-27.7679
JADES-GN+189.2707+62.1484	1038147	5.82	189.2707	62.1484	JADES-GS+53.1479-27.7599	143133	6.43	53.1479	-27.7599
JADES-GN+189.2062+62.1505	1038673	6.43	189.2062	62.1505	JADES-GS+53.1582-27.7391	154428	6.54	53.1582	-27.7391
JADES-GN+189.2631+62.1512	1038849	3.91	189.2631	62.1512	JADES-GS+53.0789-27.8842	165902	5.56	53.0789	-27.8842
JADES-GN+189.2940+62.1531	1039353	5.29	189.2940	62.1531	JADES-GS+53.0877-27.8712	172975	4.78	53.0877	-27.8712
JADES-GN+189.2436+62.1549	1039805	5.26	189.2436	62.1549	JADES-GS+53.0557-27.8688	174121	7.30	53.0557	-27.8688
JADES-GN+189.2024+62.1627	1042541	5.41	189.2024	62.1627	JADES-GS+53.0374-27.8656	175930	5.35	53.0374	-27.8656
JADES-GN+189.3216+62.1627	1042550	7.45	189.3216	62.1627	JADES-GS+53.0964-27.8531	184838	7.32	53.0964	-27.8531
JADES-GN+189.2735+62.1665	1043804	5.84	189.2735	62.1665	JADES-GS+53.1060-27.8482	187025	6.92	53.1060	-27.8482
JADES-GN+189.3395+62.1848	1050323	6.89	189.3395	62.1848	JADES-GS+53.1265-27.8181	197348	5.919*	53.1265	-27.8181
JADES-GN+189.1748+62.1901	1052210	6.01	189.1748	62.1901	JADES-GS+53.0677-27.8123	198980	4.68	53.0677	-27.8123
JADES-GN+189.1493+62.2075	1058594	3.64	189.1493	62.2075	JADES-GS+53.1548-27.8065	200576	6.31	53.1548	-27.8065
JADES-GN+189.1680+62.2170	1061888	5.874*	189.1680	62.2170	JADES-GS+53.1214-27.7949	203749	7.53	53.1214	-27.7949
JADES-GN+189.2248+62.2258	1064405	5.20	189.2248	62.2258	JADES-GS+53.1135-27.7935	204022	7.45	53.1135	-27.7935
JADES-GN+189.2613+62.2320	1065744	5.56	189.2613	62.2320	JADES-GS+53.1386-27.7903	204851	5.42	53.1386	-27.7903
JADES-GN+189.2292+62.1462	1068797	5.06	189.2292	62.1462	JADES-GS+53.1390-27.7844	206858	3.941*	53.1390	-27.7844
JADES-GN+189.2141+62.1490	1069100	5.44	189.2141	62.1490	JADES-GS+53.1661-27.7720	210600	6.310*	53.1661	-27.7720
JADES-GN+189.2793+62.1501	1069299	5.47	189.2793	62.1501	JADES-GS+53.1792-27.7587	214552	5.97	53.1792	-27.7587
JADES-GN+189.2358+62.1681	1072112	5.43	189.2358	62.1681	JADES-GS+53.1925-27.7531	216165	5.99	53.1925	-27.7531
JADES-GN+189.1974+62.1772	1073488	4.132*	189.1974	62.1772	JADES-GS+53.1848-27.7440	217926	6.97	53.1848	-27.7440
JADES-GN+189.3075+62.1780	1073625	6.23	189.3075	62.1780	JADES-GS+53.1583-27.7409	218515	5.98	53.1583	-27.7409
JADES-GN+189.1786+62.1872	1075363	5.44	189.1786	62.1872	JADES-GS+53.1614-27.7377	219000	6.85	53.1614	-27.7377
JADES-GN+189.1493+62.2083	1079572	3.966*	189.1493	62.2083	JADES-GS+53.1248-27.8663	283663	4.55	53.1248	-27.8663
JADES-GN+189.2816+62.2161	1081040	4.85	189.2816	62.2161	—	—	—	—	—
JADES-GN+189.2854+62.2235	1081928	6.27	189.2854	62.2235	—	—	—	—	—
JADES-GN+189.0962+62.2392	1113205	7.40	189.0962	62.2392	—	—	—	—	—
JADES-GN+189.2143+62.1491	1119051	5.44	189.2143	62.1491	—	—	—	—	—
JADES-GN+189.1364+62.2226	1177425	7.03	189.1364	62.2226	—	—	—	—	—

NOTE—Sources with spectroscopic redshifts (z_{spec}) are marked with * (Bunker et al. 2023; D’Eugenio et al. 2024). Photometric redshifts come from EAZY (Hainline et al. 2024b).

Table 2. Morphological parameters for the LRDs with enough SNR for morphological analysis

NIRCam ID	$r_{\max, \text{circ}}$	SNR/pixel	A_s	S	M	I	D
204851	16.812	6.601	0.63	-0.181	0.889	0.855	0.151
1010816	11.789	4.976	1.174	-0.216	0.200	0.535	0.113
1017514	10.273	5.150	0.323	-0.266	0.500	0.000	0.055
1020140	9.550	4.881	0.353	-0.224	0.011	0.000	0.068
1029154	24.500	5.502	1.125	-0.126	0.849	0.463	0.270
1033797	8.102	4.817	0.358	-0.194	0.037	0.000	0.033
1038147	11.290	6.207	0.499	-0.205	0.048	0.000	0.120
1050323	17.429	7.259	0.399	-0.204	0.097	0.084	0.076
1052210	14.091	8.728	0.575	-0.161	0.125	0.225	0.006
1058594	12.899	9.284	0.445	-0.146	0.281	0.000	0.284
1065744	7.288	6.868	0.201	-0.211	0.015	0.000	0.008
1069100	19.202	9.082	0.624	-0.102	0.563	0.415	0.371
1069299	8.346	6.448	0.349	-0.323	0.292	0.274	0.389
1073488	9.254	7.925	0.488	-0.165	0.148	0.000	0.046
1079572	16.946	6.879	0.554	-0.189	0.913	0.682	0.543
1081040	20.154	8.842	0.527	-0.134	0.476	0.233	0.165
1119051	19.132	7.996	0.645	-0.111	0.563	0.418	0.335
11786	12.261	6.578	1.296	-0.240	1.000	0.593	0.128
13418	9.789	6.157	0.673	-0.212	0.034	0.000	0.010
172975	5.469	11.249	0.251	-0.196	0.077	0.000	0.036
174121	11.834	7.065	0.746	-0.236	0.368	0.303	0.090
175930	17.884	12.833	0.836	-0.109	0.100	0.000	0.075
187025	16.514	6.968	0.875	-0.261	0.154	0.000	0.162
19348	5.347	5.289	0.390	-0.208	0.000	0.000	0.054
197348	9.392	9.392	0.679	-0.267	0.071	0.000	0.068
206858	27.303	12.626	0.521	-0.072	0.681	0.509	0.332
210600	8.852	11.807	0.413	-0.187	0.071	0.000	0.019
214552	14.834	11.758	0.635	-0.159	0.189	0.246	0.087
219000	6.522	9.998	0.193	-0.103	0.000	0.000	0.146
79803	7.437	6.527	0.280	-0.225	1.000	0.980	0.103

NOTE—This table lists morphological parameters extracted from STARMORPH for the LRD with sufficient SNR for robust morphological analysis. Columns include the maximum circular radius $r_{\max, \text{circ}}$, SNR per pixel, shape asymmetry (A_s), smoothness (S), multiplicity (M), intensity (I), and deviation (D).

Table 3. Emission Line Measurements for LRDs with NIRSPEC data

NIRCam ID	[O III] λ 5007 (10^{-20} erg/s/cm 2)	H β (10^{-20} erg/s/cm 2)	[Ne III] λ 3870 (10^{-20} erg/s/cm 2)	[O II] λ 3727 (10^{-20} erg/s/cm 2)	H γ (10^{-20} erg/s/cm 2)	[O III] λ 4363 (10^{-20} erg/s/cm 2)
197348	454.93 \pm 9.19	82.06 \pm 1.71	33.63 \pm 2.19	16.60 \pm 4.60	—	—
110739	744.32 \pm 11.30	167.73 \pm 13.23	65.33 \pm 13.37	61.43 \pm 9.53	82.37 \pm 15.76	51.02 \pm 19.41
206858	594.88 \pm 27.17	160.08 \pm 11.82	33.40 \pm 23.90	102.21 \pm 31.84	2.84 \pm 1.86*	18.15 \pm 18.53*
210600	723.67 \pm 41.44	98.51 \pm 4.85	34.09 \pm 6.94	64.45 \pm 11.85	—	—
1010816	1200.75 \pm 22.27	146.24 \pm 8.46	109.16 \pm 9.90	103.10 \pm 55.01*	59.46 \pm 11.19	68.35 \pm 18.46
1001093	226.02 \pm 8.77	62.44 \pm 11.59	54.70 \pm 17.70	4.99 \pm 15.09*	17.22 \pm 9.77*	6.95 \pm 7.45*
1001830	531.57 \pm 14.61	73.80 \pm 14.83	53.12 \pm 7.66	14.75 \pm 8.54	21.89 \pm 8.22	10.52 \pm 12.32*
1004685	84.27 \pm 7.88	51.27 \pm 8.29	17.30 \pm 4.76	4.96 \pm 8.28*	19.58 \pm 5.00	7.63 \pm 4.67*
1013041	918.91 \pm 18.09	153.56 \pm 7.42	37.59 \pm 11.85	14.85 \pm 9.16*	67.78 \pm 8.45	48.49 \pm 9.70
1032447	1231.22 \pm 20.99	197.28 \pm 16.30	101.14 \pm 10.06	51.55 \pm 11.74	55.17 \pm 18.15	60.27 \pm 17.16
1034762	298.76 \pm 11.13	60.08 \pm 10.63	35.04 \pm 7.15	48.28 \pm 14.29	38.36 \pm 14.20	—
1061888	283.32 \pm 7.26	89.99 \pm 7.77	23.03 \pm 10.33	12.29 \pm 5.91	109.07 \pm 17.45	18.80 \pm 11.50*
1073488	1161.28 \pm 14.23	223.88 \pm 28.73	103.35 \pm 25.05	56.44 \pm 18.47	145.62 \pm 12.02	88.34 \pm 14.60
1079572	680.03 \pm 18.51	137.64 \pm 15.40	83.01 \pm 20.43	106.93 \pm 23.94	109.61 \pm 15.76	71.11 \pm 25.83

NOTE—Emission line measurements are given as the flux \pm error in units of 10^{-20} erg/s/cm 2 . Sources with * have SNR $<$ 2 for the respective line.

8. APPENDIX A

Here we present the mathematical formalisms underpinning the *Multimode-Intensity-Deviation* (*MID*) and *shape asymmetry* A_S morphology indicators chosen to characterize the LRDs of the present study. We utilized the STATMORPH code for the morphology analysis, which reads a galaxy image and its associated weight map (the 1σ error image, also known as the ‘sigma image’ in Galfit and similar image analyses) to examine both the brightness and spatial distribution of its pixel values. It then calculates various galaxy morphology metrics, including the following non-parametric measures of galaxy structure: asymmetry (A), clumpiness (S), concentration index (C), Gini index (G), and moment of light (M20) (Lotz et al. 2004, Wu 1999, Bershadsky et al. 2000, Conselice et al. 2000. STATMORPH computes the *MID* and A_S statistics as detailed below, with slight modifications to their original definitions as presented in Freeman et al. (2013) and Pawlik et al. (2016), respectively (Rodriguez-Gomez et al. 2019).

9. MULTIMODE-INTENSITY-DEVIATION (MID) STATISTICS

The *statmorph* software calculates the non-parametric *Multimode-Intensity-Deviation* (*MID*) statistics according to their original definitions in Freeman et al. (2013), except for the **Multimode** (**M**) statistic, for which a modified version defined in Peth et al. (2016) is adopted. The algorithm defining the M statistic locates all the non-contiguous groups of image pixels that lie above a given intensity threshold, q , sorts them by pixel area, then computes the area ratio of the second-largest group ($A_{q,2}$) to the first ($A_{q,1}$); this process is then repeated for a number of intensity thresholds. M is represented by the maximum area ratio resulting from all the trials:

$$M = \max_q (A_{q,2}/A_{q,1}) \quad (2)$$

As such, M values approaching 1 are likely to indicate a double-nucleus, while values close to zero should be interpreted as a single source (i.e., where the non-zero detection of a relatively small, secondary pixel group is likely to be noise).

The **Intensity** (**I**) statistic serves as a complement to M in that it computes the intensity ratio of the two brightest source regions in the galaxy image. It does so by first locating all the distinct intensity maxima in a smoothed image of the galaxy emission; identifying and summing the intensities of the group of pixels belonging to each intensity peak; and then calculating the ratio of the summed intensity of the second-brightest pixel group (I_2) to the first (I_1):

$$I = I_2/I_1 \quad (3)$$

It should be noted that, due to the different ways in which the M and I statistics are calculated, they may not simultaneously detect multiple sources/components of emission in a given galaxy image. In other words, M is a function of the spatial footprint of distinct regions in the galaxy emission, while I considers their relative intensities. However, this can be a useful difference in cases of relatively faint emission components/sources and/or low resolution, where one of the statistics can provide an independent, compensating measure where the other statistic fails to detect multiple image components (or confirms the finding of the other where both agree). Such a scenario could occur where M detects multiple distinct regions of emission within the galaxy image, but I does not resolve more than one local intensity maximum. There can also be a case where the I statistic locates a relatively small but bright secondary region of emission, that leads to a disproportionately small value of M .

The **Deviation** (**D**) statistic provides a measure of the normalized distance between the centroid of the total extent of the galaxy emission as identified in the segmentation map, and its brightest local intensity maximum. This statistic is therefore useful in identifying irregular/peculiar galaxy shapes – e.g. late-stage or post-coalescent mergers, or active sources experiencing significant spatial disruption from star-forming and/or AGN processes – given the expectation that symmetric and ordered morphologies such as spheroids and disks would show a D value close to zero. It is calculated according to the following formula, where the image centroid is represented by (x_c, y_c) , the brightest peak resulting from the I statistic calculation is (x_{I_1}, y_{I_1}) , and n_{seg} is the number of pixels in the segmentation map.

$$D = \sqrt{\pi/n_{seg}} \sqrt{(x_c - x_{I_1})^2 + (y_c - y_{I_1})^2} \quad (4)$$

10. SHAPE ASYMMETRY (A_S)

The A_S parameter is calculated in exactly the same way as the classic A parameter, except that it is performed on the binary detection mask as opposed to the corresponding image containing the source emission (Pawlik et al. 2016). As such, A_S traces only the spatial outline of a galaxy image, while A considers asymmetries in both the pixel intensity values and their spatial locations within the emission image. Due to the assignment of equal weights to all components of the galaxy, without regard to their relative brightness, A_S is more sensitive

to features with low surface brightness along the galaxy edges. The mathematical formalism is shown below, and essentially involves subtracting a 180-degree rotated image of the galaxy from the original image; measuring the sum of the fractional pixel intensity ($I_{i,j}$) changes due to the rotation; and then subtracting from this a measure of the average asymmetry of the background emission.

$$\mathbf{A} = \sum_{i,j} |I_{i,j} - I_{i,j}^{180}| / \sum_{i,j} |I_{i,j}| - A_{bgr} \quad (5)$$

Facilities: HST, JWST.

Software: ASTROPY (Astropy Collaboration et al. 2022), BAGPIPES (Carnall et al. 2019), MSAEXP (Brammer 2023) NUMPY (Harris et al. 2020), PANDAS (team 2024) PHOTUTILS (Bradley et al. 2016), TOPCAT (Taylor 2022).

REFERENCES

- Akins, H. B., Casey, C. M., Lambrides, E., et al. 2024, COSMOS-Web: The over-abundance and physical nature of "little red dots"—Implications for early galaxy and SMBH assembly, , publication Title: arXiv e-prints ADS Bibcode: 2024arXiv240610341A, doi:10.48550/arXiv.2406.10341. <https://ui.adsabs.harvard.edu/abs/2024arXiv240610341A>
- Alberts, S., Lyu, J., Shivaee, I., et al. 2024, SMILES Initial Data Release: Unveiling the Obscured Universe with MIRI Multi-band Imaging, , publication Title: arXiv e-prints ADS Bibcode: 2024arXiv240515972A, doi:10.48550/arXiv.2405.15972. <https://ui.adsabs.harvard.edu/abs/2024arXiv240515972A>
- Amorín, R., Pérez-Montero, E., Contini, T., et al. 2015, Astronomy and Astrophysics, 578, A105, aDS Bibcode: 2015A&A...578A.105A. <https://ui.adsabs.harvard.edu/abs/2015A&A...578A.105A>
- Astropy Collaboration, Price-Whelan, A. M., Lim, P. L., et al. 2022, The Astrophysical Journal, 935, 167, publisher: IOP ADS Bibcode: 2022ApJ...935..167A. <https://ui.adsabs.harvard.edu/abs/2022ApJ...935..167A>
- Backhaus, B. E., Trump, J. R., Cleri, N. J., et al. 2022, The Astrophysical Journal, 926, 161, publisher: IOP ADS Bibcode: 2022ApJ...926..161B. <https://ui.adsabs.harvard.edu/abs/2022ApJ...926..161B>
- Backhaus, B. E., Bridge, J. S., Trump, J. R., et al. 2023, The Astrophysical Journal, 943, 37, publisher: IOP ADS Bibcode: 2023ApJ...943...37B. <https://ui.adsabs.harvard.edu/abs/2023ApJ...943...37B>
- Backhaus, B. E., Trump, J. R., Pirzkal, N., et al. 2024, The Astrophysical Journal, 962, 195, publisher: IOP ADS Bibcode: 2024ApJ...962..195B. <https://ui.adsabs.harvard.edu/abs/2024ApJ...962..195B>
- Baggen, J. F. W., van Dokkum, P., Brammer, G., et al. 2024, The Small Sizes and High Implied Densities of 'Little Red Dots' with Balmer Breaks Could Explain Their Broad Emission Lines Without an AGN, , , publication Title: arXiv e-prints ADS Bibcode: 2024arXiv240807745B, doi:10.48550/arXiv.2408.07745. <https://ui.adsabs.harvard.edu/abs/2024arXiv240807745B>
- Bagley, M. B., Pirzkal, N., Finkelstein, S. L., et al. 2024, The Astrophysical Journal, 965, L6, publisher: IOP ADS Bibcode: 2024ApJ...965L...6B. <https://ui.adsabs.harvard.edu/abs/2024ApJ...965L...6B>
- Baldwin, J. A., Phillips, M. M., & Terlevich, R. 1981, Publications of the Astronomical Society of the Pacific, 93, 5, publisher: IOP ADS Bibcode: 1981PASP...93....5B. <https://ui.adsabs.harvard.edu/abs/1981PASP...93....5B>
- Barro, G., Pérez-González, P. G., Kocevski, D. D., et al. 2024, The Astrophysical Journal, 963, 128, publisher: IOP ADS Bibcode: 2024ApJ...963..128B. <https://ui.adsabs.harvard.edu/abs/2024ApJ...963..128B>
- Blumenthal, K. A., & Barnes, J. E. 2018, Monthly Notices of the Royal Astronomical Society, 479, 3952, publisher: OUP ADS Bibcode: 2018MNRAS.479.3952B. <https://ui.adsabs.harvard.edu/abs/2018MNRAS.479.3952B>
- Bogdan, A., Goulding, A. D., Natarajan, P., et al. 2024, Nature Astronomy, 8, 126, aDS Bibcode: 2024NatAs...8..126B. <https://ui.adsabs.harvard.edu/abs/2024NatAs...8..126B>
- Bonaventura, N., Lyu, J., Rieke, G. H., et al. 2024, The Relation Between AGN and Host Galaxy Properties: I. Obscured AGN reside in disturbed hosts at 0, , , , publication Title: arXiv e-prints ADS Bibcode: 2024arXiv240107863B, doi:10.48550/arXiv.2401.07863. <https://ui.adsabs.harvard.edu/abs/2024arXiv240107863B>

- Bouwens, R. J., Illingworth, G. D., González, V., et al. 2010, *The Astrophysical Journal*, 725, 1587, publisher: IOP ADS Bibcode: 2010ApJ...725.1587B. <https://ui.adsabs.harvard.edu/abs/2010ApJ...725.1587B>
- Boyett, K., Bunker, A. J., Curtis-Lake, E., et al. 2024, *Monthly Notices of the Royal Astronomical Society*, doi:10.1093/mnras/stae2430, publisher: OUP ADS Bibcode: 2024MNRAS.tmp.2365B. <https://ui.adsabs.harvard.edu/abs/2024MNRAS.tmp.2365B>
- Bradley, L., Sipocz, B., Robitaille, T., et al. 2016, *Astrophysics Source Code Library*, ascl:1609.011, aDS Bibcode: 2016ascl.soft09011B. <https://ui.adsabs.harvard.edu/abs/2016ascl.soft09011B>
- Bradley, L. D., Coe, D., Brammer, G., et al. 2023, *The Astrophysical Journal*, 955, 13, publisher: IOP ADS Bibcode: 2023ApJ...955...13B. <https://ui.adsabs.harvard.edu/abs/2023ApJ...955...13B>
- Brammer, G. 2023, Zenodo, doi:10.5281/zenodo.7299500, publisher: Zenodo ADS Bibcode: 2022zndo...7299500B. <https://ui.adsabs.harvard.edu/abs/2022zndo...7299500B>
- Brinchmann, J. 2023, *Monthly Notices of the Royal Astronomical Society*, 525, 2087, publisher: OUP ADS Bibcode: 2023MNRAS.525.2087B. <https://ui.adsabs.harvard.edu/abs/2023MNRAS.525.2087B>
- Bruzual, G., & Charlot, S. 2003, *Monthly Notices of the Royal Astronomical Society*, 344, 1000, publisher: OUP ADS Bibcode: 2003MNRAS.344.1000B. <https://ui.adsabs.harvard.edu/abs/2003MNRAS.344.1000B>
- Bunker, A. J., Saxena, A., Cameron, A. J., et al. 2023, *Astronomy and Astrophysics*, 677, A88, aDS Bibcode: 2023A&A...677A..88B. <https://ui.adsabs.harvard.edu/abs/2023A&A...677A..88B>
- Bunker, A. J., Cameron, A. J., Curtis-Lake, E., et al. 2024, *Astronomy and Astrophysics*, 690, A288, publisher: EDP ADS Bibcode: 2024A&A...690A.288B. <https://ui.adsabs.harvard.edu/abs/2024A&A...690A.288B>
- Buta, R. J. 2011, *Galaxy Morphology*, , , publication Title: arXiv e-prints ADS Bibcode: 2011arXiv1102.0550B, doi:10.48550/arXiv.1102.0550. <https://ui.adsabs.harvard.edu/abs/2011arXiv1102.0550B>
- Calzetti, D., Armus, L., Bohlin, R. C., et al. 2000, *The Astrophysical Journal*, 533, 682, publisher: IOP ADS Bibcode: 2000ApJ...533..682C. <https://ui.adsabs.harvard.edu/abs/2000ApJ...533..682C>
- Caputi, K. I., Rinaldi, P., Iani, E., et al. 2024, *The Astrophysical Journal*, 969, 159, publisher: IOP ADS Bibcode: 2024ApJ...969..159C. <https://ui.adsabs.harvard.edu/abs/2024ApJ...969..159C>
- Carnall, A. C., McLure, R. J., Dunlop, J. S., et al. 2019, *Monthly Notices of the Royal Astronomical Society*, 490, 417, publisher: OUP ADS Bibcode: 2019MNRAS.490..417C. <https://ui.adsabs.harvard.edu/abs/2019MNRAS.490..417C>
- . 2023, *Nature*, 619, 716, aDS Bibcode: 2023Natur.619..716C. <https://ui.adsabs.harvard.edu/abs/2023Natur.619..716C>
- Cleri, N. J., Olivier, G. M., Hutchison, T. A., et al. 2023, *The Astrophysical Journal*, 953, 10, publisher: IOP ADS Bibcode: 2023ApJ...953...10C. <https://ui.adsabs.harvard.edu/abs/2023ApJ...953...10C>
- Conselice, C. J., Chapman, S. C., & Windhorst, R. A. 2003, *The Astrophysical Journal*, 596, L5, publisher: IOP ADS Bibcode: 2003ApJ...596L...5C. <https://ui.adsabs.harvard.edu/abs/2003ApJ...596L...5C>
- Cox, T. J., Di Matteo, T., Hernquist, L., et al. 2006, *The Astrophysical Journal*, 643, 692, publisher: IOP ADS Bibcode: 2006ApJ...643..692C. <https://ui.adsabs.harvard.edu/abs/2006ApJ...643..692C>
- Curti, M., D'Eugenio, F., Carniani, S., et al. 2023, *Monthly Notices of the Royal Astronomical Society*, 518, 425, publisher: OUP ADS Bibcode: 2023MNRAS.518..425C. <https://ui.adsabs.harvard.edu/abs/2023MNRAS.518..425C>
- DeGraf, C., Dekel, A., Gabor, J., & Bournaud, F. 2017, *Monthly Notices of the Royal Astronomical Society*, 466, 1462, publisher: OUP ADS Bibcode: 2017MNRAS.466.1462D. <https://ui.adsabs.harvard.edu/abs/2017MNRAS.466.1462D>
- Desprez, G., Martis, N. S., Asada, Y., et al. 2024, *Monthly Notices of the Royal Astronomical Society*, 530, 2935, publisher: OUP ADS Bibcode: 2024MNRAS.530.2935D. <https://ui.adsabs.harvard.edu/abs/2024MNRAS.530.2935D>
- D'Eugenio, F., Cameron, A. J., Scholtz, J., et al. 2024, *JADES Data Release 3 – NIRSpec/MSA spectroscopy for 4,000 galaxies in the GOODS fields*, , , publication Title: arXiv e-prints ADS Bibcode: 2024arXiv240406531D, doi:10.48550/arXiv.2404.06531. <https://ui.adsabs.harvard.edu/abs/2024arXiv240406531D>
- Duan, Q., Li, Q., Conselice, C. J., et al. 2024, *Galaxy Mergers in the Epoch of Reionization II: Major Merger-Triggered Star Formation and AGN Activities at $z = 4.5 - 8.5$* , , , publication Title: arXiv e-prints ADS Bibcode: 2024arXiv241104944D, doi:10.48550/arXiv.2411.04944. <https://ui.adsabs.harvard.edu/abs/2024arXiv241104944D>

- Durodola, E., Pacucci, F., & Hickox, R. C. 2024, Exploring the AGN Fraction of a Sample of JWST's Little Red Dots at $5 < z < 8$: Overmassive Black Holes Are Strongly Favored, , , publication Title: arXiv e-prints ADS Bibcode: 2024arXiv240610329D, doi:10.48550/arXiv.2406.10329. <https://ui.adsabs.harvard.edu/abs/2024arXiv240610329D>
- Eisenstein, D. J., Willott, C., Alberts, S., et al. 2023a, Overview of the JWST Advanced Deep Extragalactic Survey (JADES), , , publication Title: arXiv e-prints ADS Bibcode: 2023arXiv230602465E, doi:10.48550/arXiv.2306.02465. <https://ui.adsabs.harvard.edu/abs/2023arXiv230602465E>
- Eisenstein, D. J., Johnson, B. D., Robertson, B., et al. 2023b, The JADES Origins Field: A New JWST Deep Field in the JADES Second NIRCам Data Release, , , publication Title: arXiv e-prints ADS Bibcode: 2023arXiv231012340E, doi:10.48550/arXiv.2310.12340. <https://ui.adsabs.harvard.edu/abs/2023arXiv231012340E>
- Ellison, S. L., Viswanathan, A., Patton, D. R., et al. 2019, Monthly Notices of the Royal Astronomical Society, 487, 2491, publisher: OUP ADS Bibcode: 2019MNRAS.487.2491E. <https://ui.adsabs.harvard.edu/abs/2019MNRAS.487.2491E>
- Endsley, R., Stark, D. P., Whittler, L., et al. 2023, Monthly Notices of the Royal Astronomical Society, 524, 2312, publisher: OUP ADS Bibcode: 2023MNRAS.524.2312E. <https://ui.adsabs.harvard.edu/abs/2023MNRAS.524.2312E>
- . 2024, Monthly Notices of the Royal Astronomical Society, 533, 1111, publisher: OUP ADS Bibcode: 2024MNRAS.533.1111E. <https://ui.adsabs.harvard.edu/abs/2024MNRAS.533.1111E>
- Feltre, A., Charlot, S., & Gutkin, J. 2016, Monthly Notices of the Royal Astronomical Society, 456, 3354, publisher: OUP ADS Bibcode: 2016MNRAS.456.3354F. <https://ui.adsabs.harvard.edu/abs/2016MNRAS.456.3354F>
- Ferland, G. J., Porter, R. L., van Hoof, P. A. M., et al. 2013, Revista Mexicana de Astronomía y Astrofísica, 49, 137, aDS Bibcode: 2013RMxAA..49..137F. <https://ui.adsabs.harvard.edu/abs/2013RMxAA..49..137F>
- Feuillet, L. M., Meléndez, M., Kraemer, S., et al. 2024, The Astrophysical Journal, 962, 104, publisher: IOP ADS Bibcode: 2024ApJ...962..104F. <https://ui.adsabs.harvard.edu/abs/2024ApJ...962..104F>
- Freeman, P. E., Izbicki, R., Lee, A. B., et al. 2013, Monthly Notices of the Royal Astronomical Society, 434, 282, publisher: OUP ADS Bibcode: 2013MNRAS.434..282F. <https://ui.adsabs.harvard.edu/abs/2013MNRAS.434..282F>
- Furtak, L. J., Zitrin, A., Plat, A., et al. 2023, The Astrophysical Journal, 952, 142, publisher: IOP ADS Bibcode: 2023ApJ...952..142F. <https://ui.adsabs.harvard.edu/abs/2023ApJ...952..142F>
- Furtak, L. J., Labbé, I., Zitrin, A., et al. 2024, Nature, 628, 57, aDS Bibcode: 2024Natur.628...57F. <https://ui.adsabs.harvard.edu/abs/2024Natur.628...57F>
- Gabor, J. M., Capelo, P. R., Volonteri, M., et al. 2016, Astronomy and Astrophysics, 592, A62, aDS Bibcode: 2016A&A...592A..62G. <https://ui.adsabs.harvard.edu/abs/2016A&A...592A..62G>
- Gardner, J. P., Mather, J. C., Abbott, R., et al. 2023, Publications of the Astronomical Society of the Pacific, 135, 068001, publisher: IOP ADS Bibcode: 2023PASP..135f8001G. <https://ui.adsabs.harvard.edu/abs/2023PASP..135f8001G>
- Gburek, T., Siana, B., Alavi, A., et al. 2019, The Astrophysical Journal, 887, 168, publisher: IOP ADS Bibcode: 2019ApJ...887..168G. <https://ui.adsabs.harvard.edu/abs/2019ApJ...887..168G>
- Giavalisco, M., Ferguson, H. C., Koekemoer, A. M., et al. 2004, The Astrophysical Journal, 600, L93, publisher: IOP ADS Bibcode: 2004ApJ...600L..93G. <https://ui.adsabs.harvard.edu/abs/2004ApJ...600L..93G>
- Greene, J. E., Strader, J., & Ho, L. C. 2020, Annual Review of Astronomy and Astrophysics, 58, 257, aDS Bibcode: 2020ARA&A..58..257G. <https://ui.adsabs.harvard.edu/abs/2020ARA&A..58..257G>
- Greene, J. E., Seth, A., Kim, M., et al. 2016, The Astrophysical Journal, 826, L32, publisher: IOP ADS Bibcode: 2016ApJ...826L..32G. <https://ui.adsabs.harvard.edu/abs/2016ApJ...826L..32G>
- Greene, J. E., Labbe, I., Goulding, A. D., et al. 2024, The Astrophysical Journal, 964, 39, publisher: IOP ADS Bibcode: 2024ApJ...964...39G. <https://ui.adsabs.harvard.edu/abs/2024ApJ...964...39G>
- Guo, Y., Ferguson, H. C., Bell, E. F., et al. 2015, The Astrophysical Journal, 800, 39, publisher: IOP ADS Bibcode: 2015ApJ...800...39G. <https://ui.adsabs.harvard.edu/abs/2015ApJ...800...39G>
- Gutkin, J., Charlot, S., & Bruzual, G. 2016, Monthly Notices of the Royal Astronomical Society, 462, 1757, publisher: OUP ADS Bibcode: 2016MNRAS.462.1757G. <https://ui.adsabs.harvard.edu/abs/2016MNRAS.462.1757G>

- Hainline, K. N., Maiolino, R., Juodzbališ, I., et al. 2024a, An Investigation Into The Selection and Colors of Little Red Dots and Active Galactic Nuclei, , , publication Title: arXiv e-prints ADS Bibcode: 2024arXiv241000100H, doi:10.48550/arXiv.2410.00100. <https://ui.adsabs.harvard.edu/abs/2024arXiv241000100H>
- Hainline, K. N., Johnson, B. D., Robertson, B., et al. 2024b, The Astrophysical Journal, 964, 71, publisher: IOP ADS Bibcode: 2024ApJ...964...71H. <https://ui.adsabs.harvard.edu/abs/2024ApJ...964...71H>
- Harikane, Y., Zhang, Y., Nakajima, K., et al. 2023, The Astrophysical Journal, 959, 39, publisher: IOP ADS Bibcode: 2023ApJ...959...39H. <https://ui.adsabs.harvard.edu/abs/2023ApJ...959...39H>
- Harris, C. R., Millman, K. J., van der Walt, S. J., et al. 2020, Nature, 585, 357, aDS Bibcode: 2020Natur.585..357H. <https://ui.adsabs.harvard.edu/abs/2020Natur.585..357H>
- Hewlett, T., Villforth, C., Wild, V., et al. 2017, Monthly Notices of the Royal Astronomical Society, 470, 755, publisher: OUP ADS Bibcode: 2017MNRAS.470..755H. <https://ui.adsabs.harvard.edu/abs/2017MNRAS.470..755H>
- Iani, E., Rinaldi, P., Caputi, K. I., et al. 2024, MIDIS: MIRI uncovers Virgil, an extended source at $z \sim 6.6$ with the photometric properties of Little Red Dots, , , publication Title: arXiv e-prints ADS Bibcode: 2024arXiv240618207I, doi:10.48550/arXiv.2406.18207. <https://ui.adsabs.harvard.edu/abs/2024arXiv240618207I>
- Izotov, Y. I., Thuan, T. X., & Guseva, N. G. 2007, The Astrophysical Journal, 671, 1297, publisher: IOP ADS Bibcode: 2007ApJ...671.1297I. <https://ui.adsabs.harvard.edu/abs/2007ApJ...671.1297I>
- Juodzbališ, I., Maiolino, R., Baker, W. M., et al. 2024, A dormant, overmassive black hole in the early Universe, , , publication Title: arXiv e-prints ADS Bibcode: 2024arXiv240303872J, doi:10.48550/arXiv.2403.03872. <https://ui.adsabs.harvard.edu/abs/2024arXiv240303872J>
- Killi, M., Watson, D., Brammer, G., et al. 2023, Deciphering the JWST spectrum of a 'little red dot' at $z \sim 4.53$: An obscured AGN and its star-forming host, , , publication Title: arXiv e-prints ADS Bibcode: 2023arXiv231203065K, doi:10.48550/arXiv.2312.03065. <https://ui.adsabs.harvard.edu/abs/2023arXiv231203065K>
- Kocevski, D. D., Onoue, M., Inayoshi, K., et al. 2023a, The Astrophysical Journal, 954, L4, publisher: IOP ADS Bibcode: 2023ApJ...954L...4K. <https://ui.adsabs.harvard.edu/abs/2023ApJ...954L...4K>
- Kocevski, D. D., Barro, G., McGrath, E. J., et al. 2023b, The Astrophysical Journal, 946, L14, publisher: IOP ADS Bibcode: 2023ApJ...946L..14K. <https://ui.adsabs.harvard.edu/abs/2023ApJ...946L..14K>
- Kocevski, D. D., Finkelstein, S. L., Barro, G., et al. 2024, The Rise of Faint, Red AGN at $z > 4$: A Sample of Little Red Dots in the JWST Extragalactic Legacy Fields, , , publication Title: arXiv e-prints ADS Bibcode: 2024arXiv240403576K, doi:10.48550/arXiv.2404.03576. <https://ui.adsabs.harvard.edu/abs/2024arXiv240403576K>
- Kokorev, V., Fujimoto, S., Labbe, I., et al. 2023, The Astrophysical Journal, 957, L7, publisher: IOP ADS Bibcode: 2023ApJ...957L...7K. <https://ui.adsabs.harvard.edu/abs/2023ApJ...957L...7K>
- Kokorev, V., Caputi, K. I., Greene, J. E., et al. 2024a, The Astrophysical Journal, 968, 38, publisher: IOP ADS Bibcode: 2024ApJ...968...38K. <https://ui.adsabs.harvard.edu/abs/2024ApJ...968...38K>
- Kokorev, V., Chisholm, J., Endsley, R., et al. 2024b, Silencing the Giant: Evidence of AGN Feedback and Quenching in a Little Red Dot at $z = 4.13$, , , publication Title: arXiv e-prints ADS Bibcode: 2024arXiv240720320K, doi:10.48550/arXiv.2407.20320. <https://ui.adsabs.harvard.edu/abs/2024arXiv240720320K>
- Kokubo, M., & Harikane, Y. 2024, Challenging the AGN scenario for JWST/NIRSpec broad H α emitters/Little Red Dots in light of non-detection of NIRCcam photometric variability and X-ray, , , publication Title: arXiv e-prints ADS Bibcode: 2024arXiv240704777K, doi:10.48550/arXiv.2407.04777. <https://ui.adsabs.harvard.edu/abs/2024arXiv240704777K>
- Kroupa, P. 2001, Monthly Notices of the Royal Astronomical Society, 322, 231, publisher: OUP ADS Bibcode: 2001MNRAS.322..231K. <https://ui.adsabs.harvard.edu/abs/2001MNRAS.322..231K>
- Labbé, I., van Dokkum, P., Nelson, E., et al. 2023a, Nature, 616, 266, aDS Bibcode: 2023Natur.616..266L. <https://ui.adsabs.harvard.edu/abs/2023Natur.616..266L>
- Labbé, I., Greene, J. E., Bezanson, R., et al. 2023b, UNCOVER: Candidate Red Active Galactic Nuclei at $z > 3$, , , publication Title: arXiv e-prints ADS Bibcode: 2023arXiv230607320L, doi:10.48550/arXiv.2306.07320. <https://ui.adsabs.harvard.edu/abs/2023arXiv230607320L>
- Larson, R. L., Finkelstein, S. L., Kocevski, D. D., et al. 2023, The Astrophysical Journal, 953, L29, publisher: IOP ADS Bibcode: 2023ApJ...953L..29L. <https://ui.adsabs.harvard.edu/abs/2023ApJ...953L..29L>

- Leja, J., Carnall, A. C., Johnson, B. D., Conroy, C., & Speagle, J. S. 2019, *The Astrophysical Journal*, 876, 3, publisher: IOP ADS Bibcode: 2019ApJ...876....3L. <https://ui.adsabs.harvard.edu/abs/2019ApJ...876....3L>
- Lotz, J. M., Primack, J., & Madau, P. 2004, *The Astronomical Journal*, 128, 163, publisher: IOP ADS Bibcode: 2004AJ....128..163L. <https://ui.adsabs.harvard.edu/abs/2004AJ....128..163L>
- Lyu, J., Alberts, S., Rieke, G. H., & Rujopakarn, W. 2022, *The Astrophysical Journal*, 941, 191, publisher: IOP ADS Bibcode: 2022ApJ...941..191L. <https://ui.adsabs.harvard.edu/abs/2022ApJ...941..191L>
- Lyu, J., Alberts, S., Rieke, G. H., et al. 2024, *The Astrophysical Journal*, 966, 229, publisher: IOP ADS Bibcode: 2024ApJ...966..229L. <https://ui.adsabs.harvard.edu/abs/2024ApJ...966..229L>
- Mager, V. A., Conselice, C. J., Seibert, M., et al. 2018, *The Astrophysical Journal*, 864, 123, publisher: IOP ADS Bibcode: 2018ApJ...864..123M. <https://ui.adsabs.harvard.edu/abs/2018ApJ...864..123M>
- Maiolino, R., Scholtz, J., Curtis-Lake, E., et al. 2023, JADES. The diverse population of infant Black Holes at 4, , , publication Title: arXiv e-prints ADS Bibcode: 2023arXiv230801230M, doi:10.48550/arXiv.2308.01230. <https://ui.adsabs.harvard.edu/abs/2023arXiv230801230M>
- Maiolino, R., Scholtz, J., Witstok, J., et al. 2024a, *Nature*, 627, 59, aDS Bibcode: 2024Natur.627...59M. <https://ui.adsabs.harvard.edu/abs/2024Natur.627...59M>
- Maiolino, R., Risaliti, G., Signorini, M., et al. 2024b, JWST meets Chandra: a large population of Compton thick, feedback-free, and X-ray weak AGN, with a sprinkle of SNe, , , publication Title: arXiv e-prints ADS Bibcode: 2024arXiv240500504M, doi:10.48550/arXiv.2405.00504. <https://ui.adsabs.harvard.edu/abs/2024arXiv240500504M>
- Matsuoka, Y., Onoue, M., Kashikawa, N., et al. 2019, *The Astrophysical Journal*, 872, L2, publisher: IOP ADS Bibcode: 2019ApJ...872L...2M. <https://ui.adsabs.harvard.edu/abs/2019ApJ...872L...2M>
- Matthee, J., Naidu, R. P., Brammer, G., et al. 2024, *The Astrophysical Journal*, 963, 129, publisher: IOP ADS Bibcode: 2024ApJ...963..129M. <https://ui.adsabs.harvard.edu/abs/2024ApJ...963..129M>
- Mazzolari, G., Übler, H., Maiolino, R., et al. 2024, New AGN diagnostic diagrams based on the [OIII] λ 4363 auroral line, , , publication Title: arXiv e-prints ADS Bibcode: 2024arXiv240410811M, doi:10.48550/arXiv.2404.10811. <https://ui.adsabs.harvard.edu/abs/2024arXiv240410811M>
- Nakajima, K., & Maiolino, R. 2022, *Monthly Notices of the Royal Astronomical Society*, 513, 5134, publisher: OUP ADS Bibcode: 2022MNRAS.513.5134N. <https://ui.adsabs.harvard.edu/abs/2022MNRAS.513.5134N>
- Nakajima, K., Ouchi, M., Isobe, Y., et al. 2023, *The Astrophysical Journal Supplement Series*, 269, 33, publisher: IOP ADS Bibcode: 2023ApJS..269...33N. <https://ui.adsabs.harvard.edu/abs/2023ApJS..269...33N>
- Navarro-Carrera, R., Caputi, K. I., Iani, E., et al. 2024, The interstellar medium conditions of a strong Ly α emitter at $z = 8.279$ revealed by JWST: a robust LyC leaker candidate at the Epoch of Reionization, , , publication Title: arXiv e-prints ADS Bibcode: 2024arXiv240714201N, doi:10.48550/arXiv.2407.14201. <https://ui.adsabs.harvard.edu/abs/2024arXiv240714201N>
- Nevin, R., Blecha, L., Comerford, J., & Greene, J. 2019, *The Astrophysical Journal*, 872, 76, publisher: IOP ADS Bibcode: 2019ApJ...872...76N. <https://ui.adsabs.harvard.edu/abs/2019ApJ...872...76N>
- Oesch, P. A., Brammer, G., van Dokkum, P. G., et al. 2016, *The Astrophysical Journal*, 819, 129, publisher: IOP ADS Bibcode: 2016ApJ...819..129O. <https://ui.adsabs.harvard.edu/abs/2016ApJ...819..129O>
- Oesch, P. A., Brammer, G., Naidu, R. P., et al. 2023, *Monthly Notices of the Royal Astronomical Society*, 525, 2864, publisher: OUP ADS Bibcode: 2023MNRAS.525.2864O. <https://ui.adsabs.harvard.edu/abs/2023MNRAS.525.2864O>
- Oke, J. B., & Gunn, J. E. 1983, *The Astrophysical Journal*, 266, 713, publisher: IOP ADS Bibcode: 1983ApJ...266..713O. <https://ui.adsabs.harvard.edu/abs/1983ApJ...266..713O>
- Pacucci, F., Nguyen, B., Carniani, S., Maiolino, R., & Fan, X. 2023, *The Astrophysical Journal*, 957, L3, publisher: IOP ADS Bibcode: 2023ApJ...957L...3P. <https://ui.adsabs.harvard.edu/abs/2023ApJ...957L...3P>
- Parlanti, E., Carniani, S., Übler, H., et al. 2024, *Astronomy and Astrophysics*, 684, A24, aDS Bibcode: 2024A&A...684A..24P. <https://ui.adsabs.harvard.edu/abs/2024A&A...684A..24P>
- Pawlik, M. M., Wild, V., Walcher, C. J., et al. 2016, *Monthly Notices of the Royal Astronomical Society*, 456, 3032, publisher: OUP ADS Bibcode: 2016MNRAS.456.3032P. <https://ui.adsabs.harvard.edu/abs/2016MNRAS.456.3032P>
- Pierce, J. C. S., Tadhunter, C., Ramos Almeida, C., et al. 2023, *Monthly Notices of the Royal Astronomical Society*, 522, 1736, publisher: OUP ADS Bibcode: 2023MNRAS.522.1736P. <https://ui.adsabs.harvard.edu/abs/2023MNRAS.522.1736P>

- Pérez-González, P. G., Barro, G., Annunziatella, M., et al. 2023a, *The Astrophysical Journal*, 946, L16, publisher: IOP ADS Bibcode: 2023ApJ...946L..16P. <https://ui.adsabs.harvard.edu/abs/2023ApJ...946L..16P>
- Pérez-González, P. G., Costantin, L., Langeroodi, D., et al. 2023b, *The Astrophysical Journal*, 951, L1, publisher: IOP ADS Bibcode: 2023ApJ...951L...1P. <https://ui.adsabs.harvard.edu/abs/2023ApJ...951L...1P>
- Pérez-González, P. G., Barro, G., Rieke, G. H., et al. 2024, *The Astrophysical Journal*, 968, 4, publisher: IOP ADS Bibcode: 2024ApJ...968...4P. <https://ui.adsabs.harvard.edu/abs/2024ApJ...968...4P>
- Reines, A. E., Greene, J. E., & Geha, M. 2013, *The Astrophysical Journal*, 775, 116, publisher: IOP ADS Bibcode: 2013ApJ...775..116R. <https://ui.adsabs.harvard.edu/abs/2013ApJ...775..116R>
- Richards, G. T., Lacy, M., Storrie-Lombardi, L. J., et al. 2006, *The Astrophysical Journal Supplement Series*, 166, 470, publisher: IOP ADS Bibcode: 2006ApJS..166..470R. <https://ui.adsabs.harvard.edu/abs/2006ApJS..166..470R>
- Rieke, M. J., Kelly, D. M., Misselt, K., et al. 2023, *Publications of the Astronomical Society of the Pacific*, 135, 028001, publisher: IOP ADS Bibcode: 2023PASP..135b8001R. <https://ui.adsabs.harvard.edu/abs/2023PASP..135b8001R>
- Rinaldi, P., Caputi, K. I., Costantin, L., et al. 2023, *The Astrophysical Journal*, 952, 143, publisher: IOP ADS Bibcode: 2023ApJ...952..143R. <https://ui.adsabs.harvard.edu/abs/2023ApJ...952..143R>
- Rinaldi, P., Caputi, K. I., Iani, E., et al. 2024, *The Astrophysical Journal*, 969, 12, publisher: IOP ADS Bibcode: 2024ApJ...969...12R. <https://ui.adsabs.harvard.edu/abs/2024ApJ...969...12R>
- Rodriguez-Gomez, V., Snyder, G. F., Lotz, J. M., et al. 2019, *Monthly Notices of the Royal Astronomical Society*, 483, 4140, publisher: OUP ADS Bibcode: 2019MNRAS.483.4140R. <https://ui.adsabs.harvard.edu/abs/2019MNRAS.483.4140R>
- Rubinur, K., Das, M., Kharb, P., et al. 2024, *Monthly Notices of the Royal Astronomical Society*, 528, 4432, publisher: OUP ADS Bibcode: 2024MNRAS.528.4432R. <https://ui.adsabs.harvard.edu/abs/2024MNRAS.528.4432R>
- Sanders, R. L., Shapley, A. E., Kriek, M., et al. 2016, *The Astrophysical Journal*, 825, L23, publisher: IOP ADS Bibcode: 2016ApJ...825L..23S. <https://ui.adsabs.harvard.edu/abs/2016ApJ...825L..23S>
- Scholtz, J., Maiolino, R., D'Eugenio, F., et al. 2023, *JADES: A large population of obscured, narrow line AGN at high redshift*, , publication Title: arXiv e-prints ADS Bibcode: 2023arXiv231118731S, doi:10.48550/arXiv.2311.18731. <https://ui.adsabs.harvard.edu/abs/2023arXiv231118731S>
- Shah, E. A., Kartaltepe, J. S., Magagnoli, C. T., et al. 2020, *The Astrophysical Journal*, 904, 107, publisher: IOP ADS Bibcode: 2020ApJ...904..107S. <https://ui.adsabs.harvard.edu/abs/2020ApJ...904..107S>
- Tacchella, S., Eisenstein, D. J., Hainline, K., et al. 2023, *The Astrophysical Journal*, 952, 74, publisher: IOP ADS Bibcode: 2023ApJ...952...74T. <https://ui.adsabs.harvard.edu/abs/2023ApJ...952...74T>
- Taylor, M. 2022, 532, 3, conference Name: *Astronomical Data Analysis Software and Systems XXX* ADS Bibcode: 2022ASPC..532....3T. <https://ui.adsabs.harvard.edu/abs/2022ASPC..532....3T>
- team, T. p. d. 2024, *pandas-dev/pandas: Pandas*, Zenodo, doi:10.5281/zenodo.13819579. <https://zenodo.org/records/13819579>
- Treu, T., Calabrò, A., Castellano, M., et al. 2023, *The Astrophysical Journal*, 942, L28, publisher: IOP ADS Bibcode: 2023ApJ...942L..28T. <https://ui.adsabs.harvard.edu/abs/2023ApJ...942L..28T>
- Tripodi, R., D'Eugenio, F., Maiolino, R., et al. 2024, *Spatially resolved emission lines in galaxies at $4 < \log z < 10$ from the JADES survey: evidence for enhanced central star formation*, , publication Title: arXiv e-prints ADS Bibcode: 2024arXiv240308431T, doi:10.48550/arXiv.2403.08431. <https://ui.adsabs.harvard.edu/abs/2024arXiv240308431T>
- Trouille, L., Barger, A., & Tremonti, C. 2011, 217, 326.03, conference Name: *American Astronomical Society Meeting Abstracts #217* ADS Bibcode: 2011AAS...21732603T. <https://ui.adsabs.harvard.edu/abs/2011AAS...21732603T>
- Trump, J. R., Arrabal Haro, P., Simons, R. C., et al. 2023, *The Astrophysical Journal*, 945, 35, publisher: IOP ADS Bibcode: 2023ApJ...945...35T. <https://ui.adsabs.harvard.edu/abs/2023ApJ...945...35T>
- Villforth, C., Hamann, F., Rosario, D. J., et al. 2014, *Monthly Notices of the Royal Astronomical Society*, 439, 3342, publisher: OUP ADS Bibcode: 2014MNRAS.439.3342V. <https://ui.adsabs.harvard.edu/abs/2014MNRAS.439.3342V>
- Whitaker, K. E., Ashas, M., Illingworth, G., et al. 2019, *The Astrophysical Journal Supplement Series*, 244, 16, publisher: IOP ADS Bibcode: 2019ApJS..244...16W. <https://ui.adsabs.harvard.edu/abs/2019ApJS..244...16W>

- Williams, C. C., Tacchella, S., Maseda, M. V., et al. 2023, The Astrophysical Journal Supplement Series, 268, 64, publisher: IOP ADS Bibcode: 2023ApJS..268...64W. <https://ui.adsabs.harvard.edu/abs/2023ApJS..268...64W>
- Williams, C. C., Alberts, S., Ji, Z., et al. 2024, The Astrophysical Journal, 968, 34, publisher: IOP ADS Bibcode: 2024ApJ...968...34W. <https://ui.adsabs.harvard.edu/abs/2024ApJ...968...34W>
- Wright, G. S., Rieke, G. H., Glasse, A., et al. 2023, Publications of the Astronomical Society of the Pacific, 135, 048003, publisher: IOP ADS Bibcode: 2023PASP..135d8003W. <https://ui.adsabs.harvard.edu/abs/2023PASP..135d8003W>
- York, D. G., Adelman, J., Anderson, Jr., J. E., et al. 2000, The Astronomical Journal, 120, 1579, publisher: IOP ADS Bibcode: 2000AJ....120.1579Y. <https://ui.adsabs.harvard.edu/abs/2000AJ....120.1579Y>
- Yue, M., Eilers, A.-C., Ananna, T. T., et al. 2024, Stacking X-ray Observations of "Little Red Dots": Implications for their AGN Properties, , , publication Title: arXiv e-prints ADS Bibcode: 2024arXiv240413290Y, doi:10.48550/arXiv.2404.13290. <https://ui.adsabs.harvard.edu/abs/2024arXiv240413290Y>
- Zeimann, G. R., Ciardullo, R., Gebhardt, H., et al. 2015, The Astrophysical Journal, 798, 29, publisher: IOP ADS Bibcode: 2015ApJ...798...29Z. <https://ui.adsabs.harvard.edu/abs/2015ApJ...798...29Z>
- Übler, H., Maiolino, R., Curtis-Lake, E., et al. 2023, Astronomy and Astrophysics, 677, A145, aDS Bibcode: 2023A&A...677A.145U. <https://ui.adsabs.harvard.edu/abs/2023A&A...677A.145U>
- Übler, H., Maiolino, R., Pérez-González, P. G., et al. 2024, Monthly Notices of the Royal Astronomical Society, 531, 355, publisher: OUP ADS Bibcode: 2024MNRAS.531..355U. <https://ui.adsabs.harvard.edu/abs/2024MNRAS.531..355U>